

**CHARACTERIZATION OF TiO<sub>2</sub> (TITANIUM DIOXIDE)  
NANO-PARTICLE FILLED EPOXY ADHESIVE  
AND ITS METALLIC JOINT**

**A DISSERTATION**

*Submitted in partial fulfillment of the  
requirements for the award of the degree*

*of*

**MASTER OF TECHNOLOGY**

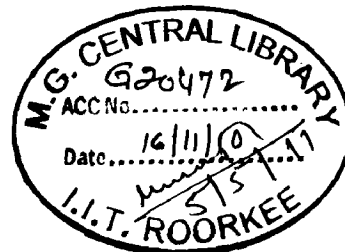
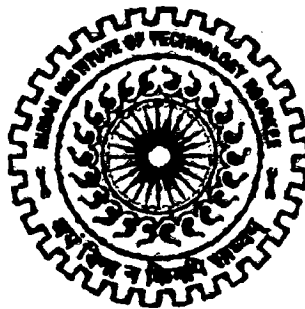
*in*

**METALLURGICAL & MATERIALS ENGINEERING**

**(With Specialization in Industrial Metallurgy)**

**By**

**ABHISHEK SUBHASHBHAI PATHAK**



**DEPARTMENT OF METALLURGICAL & MATERIALS ENGINEERING  
INDIAN INSTITUTE OF TECHNOLOGY ROORKEE  
ROORKEE - 247 667 (INDIA)  
JUNE, 2010**

### Candidate's Declaration

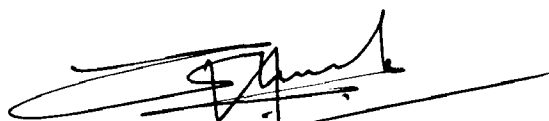
I hereby declare that the work which is being presented in the project entitled "CHARACTERIZATION OF TiO<sub>2</sub> (TITANIUM DIOXIDE) NANO PARTICLE FILLED EPOXY ADHESIVE AND ITS METALLIC JOINT" in partial fulfillment of the requirement for the award of the degree of Master of Technology in Industrial Metallurgy, submitted in Department of Metallurgical and Materials Engineering, Indian Institute of Technology, Roorkee is an authentic record of my own work carried out for the period from July 2009 to May 2010 under the supervision of Dr. P.K. Ghosh, Professor & Dr. Devendra Singh, Assistant Professor at the Department of Metallurgical and Materials Engineering, Indian Institute of Technology Roorkee. The matter embodied in this report has not been submitted by me for the award of any other degree or diploma.

Date - 30/06/2010

  
Abhishek Subhashbhai Pathak

### CERTIFICATE

This is to certify that the above statement made by the candidate is correct to the best of my knowledge.



Dr. P.K. Ghosh

Professor

Metallurgical and Materials Engg. Dept.

Indian Institute of Technology Roorkee

Roorkee – 247 667 (INDIA)



Dr. Devendra Singh

Assistant Professor

Metallurgical and Materials Engg. Dept.

Indian Institute of Technology Roorkee

Roorkee – 247 667 (INDIA)

## **ACKNOWLEDGEMENT**

I would like to acknowledge and extend deep gratitude to my guide and Head of Department **Prof. P.K. Ghosh** for his guidance and understanding. I also want to thank **Dr. D. Singh, Mr. M.S. Goyat** and **Mr. Devkumaran** for their continuous support and help in all the matter related to project work.

I am also thankful to the non-teaching staff for their help in the laboratory work.

Abhishek Pathak

## ABSTRACT

In the present work an attempt has been made to improve the resistance to fracture, thermal stability and UV degradation of epoxy based adhesive by adding TiO<sub>2</sub> nano-particles (20 – 30 nm) as filler (ex-situ) through mechanical and ultrasonic mixing methods. A brief study on metallic joint of this composite adhesive has also been done. Characterization of the epoxy based nano-composite includes the properties like tensile strength, lap shear strength, glass transition temperature and IPDT. Results show a substantial improvement in all the properties of the epoxy nano-composite upto 20 wt% TiO<sub>2</sub> addition. Fracture behavior has been studied under SEM on tensile fracture surface of the nano filled epoxy adhesive. FTIR spectroscopy has been carried out to study the changes in bonding of epoxy adhesive due to presence of TiO<sub>2</sub> nano particles. The comparative change in resistance to UV degradation has also been studied as TiO<sub>2</sub> nano particles have ability to absorb UV radiation. Metallic Joint of the composite adhesive has been characterized by its lap shear strength and analysis of fracture surface under SEM.

*Keywords: Nano-composite, Epoxy Adhesive, TiO<sub>2</sub> filler, IPDT, Metallic Joint,*

*Thermal Property, UV degradation*

## *CONTENTS*

1. Chapter 1 : Introduction	1
2. Chapter 2 : Literature Survey	3
2.1 Adhesion	3
2.1.1 Advantages of Adhesive Bonding	3
2.1.1.1 Fabrication of Smooth Exterior Surfaces	3
2.1.1.2 Protection against Shock and Vibration Failure	3
2.1.1.3 Use of Light gauge materials	4
2.1.1.4 Joining of dissimilar materials	4
2.1.1.5 Simplified Joining of contoured or delicate parts	5
2.1.1.6 Reduced Cost of manufacture and assembly	5
2.2 Epoxy Resin	6
2.3 Araldite 2011	8
2.3.1 Key properties	8
2.3.2 Processing	8
2.4 Titanium Dioxide nano particles	9
2.5 Particulate filled polymer composite	9
2.6 Work reported in literature on TiO <sub>2</sub> polymer composite	10
2.7 Effect of Particle size, particle/matrix interface adhesion and particle Loading on mechanical properties of particulate polymer composites	14
2.7.1 Young's Modulus	14
2.7.1.1 Effect of particle size and amount	14
2.7.1.2 Effect of particle/matrix interface adhesion	14
2.7.1.3 Effect of particle loading	15
2.7.1.4 Theories for elastic modulus	15
2.7.2 Strength	16
2.7.2.1 Effect of particle size and amount	16
2.7.2.2 Effect of particle/matrix interface adhesion	16
2.7.2.3 Theories of strength	16
2.7.3 Fracture toughness	17
2.7.3.1 Effect of particle size and amount	17
2.7.3.2 Effect of particle/matrix interface adhesion	17
2.7.3.3 Theories for fracture toughness	18
2.8 Ultrasonic Cavitation Method	19
3. Chapter 3: Experimental Work	20
3.1 Characterization of titanium dioxide particles	20
3.2 Composite adhesive sample preparation (Mechanical & Ultrasonic Mixing)	20
3.2.1 Sample preparation for tensile testing	20
3.2.2 Sample preparation for Atomic Force Microscopy (AFM)	21

3.2.3 Sample preparation for DTA/TGA and FTIR	21
3.2.4 Sample preparation for Lap Shear Test	22
3.3 Tensile Testing	22
3.4 Lap Shear Testing	23
3.5 Study of Thermal properties	23
3.6 Atomic Force Microscopy	24
3.7 Fracture surface study using FE-SEM	24
3.8 Fourier Transform Infrared Spectroscopy	24
3.9 Ultraviolet degradation test	25
4. Chapter 4: Result and Discussion	26
4.1 Tensile test result for mechanical and ultrasonic mixed composite	26
4.2 Lap Shear strength results	27
4.3 Glass Transition and Integral Procedural Decomposition Temperatures	28
4.4 Atomic Force Microscopy (AFM) Results	30
4.5 Fracture surface study	41
4.6 Fourier Transform Infrared Spectroscopy Results	51
4.7 UV Degradation test results	56
5. Chapter 5: Conclusion	57
6. Chapter 6: Scope of Future Work	58
7. Chapter 7: References	59

**LIST OF FIGURES**

Figure 1	Structure of unmodified epoxy prepolymer	7
Figure 2	Ultimate tensile strength and elongation at break as a function of Weight fraction of submicron size titanium dioxide particles	10
Figure 3	Effect of different size of TiO <sub>2</sub> fillers on the strain to failure of composite	11
Figure 4	Effect of different size of TiO <sub>2</sub> fillers on the scratch indentation of composite	11
Figure 5	Static Fracture toughness K <sub>IC</sub> of composite as function of filler amount	13
Figure 6	Fracture toughness as a function of filler content	14
Figure 7	Fracture toughness as a function of filler content	20
Figure 8	TEM image of TiO <sub>2</sub> particles	20
Figure 9	Drawing of ASTM D 638-08 tensile test specimen	22
Figure 10	Details of lap shear specimen	23
Figure 11	Plot to determine IPDT	24
Figure 12	Variation of applied stress with wt.% TiO <sub>2</sub> addition	26
Figure 13	Variation of Lap Shear Strength as a function of wt.% TiO <sub>2</sub> addition for Ultrasonic Mixed samples	27
Figure 14	T <sub>g</sub> for mechanically and Ultrasonically prepared samples	28
Figure 15	IPDT variation with wt. % TiO <sub>2</sub> addition	28
Figure 16	Percentage residual weight as a function of filler amount, method of mixing and temperature	30
Figure 17	2D AFM image of pure epoxy	31
Figure 18	Line analysis of pure epoxy	31
Figure 19	3D AFM image of pure epoxy	31
Figure 20	2D AFM image of 2 wt% mech. Mixed TiO <sub>2</sub> composite	31
Figure 21	Line analysis of 2 wt% mech. Mixed TiO <sub>2</sub> composite	32
Figure 22	3D AFM image of 2 wt% mech. Mixed TiO <sub>2</sub> composite	32
Figure 23	2D AFM image of 4 wt% mech. Mixed TiO <sub>2</sub> composite	32
Figure 24	Line analysis of 4 wt% mech. Mixed TiO <sub>2</sub> composite	32
Figure 25	3D AFM image of 4 wt% mech. Mixed TiO <sub>2</sub> composite	32
Figure 26	2D AFM image of 6 wt% mech. Mixed TiO <sub>2</sub> composite	32
Figure 27	Line analysis of 6 wt% mech. Mixed TiO <sub>2</sub> composite	33
Figure 28	3D AFM image of 6 wt% mech. Mixed TiO <sub>2</sub> composite	33
Figure 29	2D AFM image of 8 wt% mech. Mixed TiO <sub>2</sub> composite	33
Figure 30	Line analysis of 8 wt% mech. Mixed TiO <sub>2</sub> composite	33
Figure 31	3D AFM image of 8 wt% mech. Mixed TiO <sub>2</sub> composite	33
Figure 32	2D AFM image of 10 wt% mech. Mixed TiO <sub>2</sub> composite	33
Figure 33	Line analysis of 10 wt% mech. Mixed TiO <sub>2</sub> composite	34
Figure 34	3D AFM image of 10 wt% mech. Mixed TiO <sub>2</sub> composite	34
Figure 35	2D AFM image of 15 wt% mech. Mixed TiO <sub>2</sub> composite	34
Figure 36	Line analysis of 15 wt% mech. Mixed TiO <sub>2</sub> composite	34
Figure 37	3D AFM image of 15 wt% mech. Mixed TiO <sub>2</sub> composite	34
Figure 38	2D AFM image of 20 wt% mech. Mixed TiO <sub>2</sub> composite	34
Figure 39	Line analysis of 20 wt% mech. Mixed TiO <sub>2</sub> composite	35

Figure 40	3D AFM image of 20 wt% mech. Mixed TiO <sub>2</sub> composite	35
Figure 42	2D AFM image of 2 wt% ultrasonically mixed TiO <sub>2</sub> composite	35
Figure 42	Line analysis of 2 wt% ultrasonically mixed TiO <sub>2</sub> composite	35
Figure 43	3D AFM image of 2 wt% ultrasonically mixed TiO <sub>2</sub> composite	35
Figure 44	2D AFM image of 4 wt% ultrasonically mixed TiO <sub>2</sub> composite	35
Figure 45	Line analysis of 4 wt% ultrasonically mixed TiO <sub>2</sub> composite	36
Figure 46	3D AFM image of 4 wt% ultrasonically mixed TiO <sub>2</sub> composite	36
Figure 47	2D AFM image of 6 wt% ultrasonically mixed TiO <sub>2</sub> composite	36
Figure 48	Line analysis of 6 wt% ultrasonically mixed TiO <sub>2</sub> composite	36
Figure 49	3D AFM image of 6 wt% ultrasonically mixed TiO <sub>2</sub> composite	36
Figure 50	2D AFM image of 8 wt% ultrasonically mixed TiO <sub>2</sub> composite	36
Figure 51	Line analysis of 8 wt% ultrasonically mixed TiO <sub>2</sub> composite	37
Figure 52	3D AFM image of 8 wt% ultrasonically mixed TiO <sub>2</sub> composite	37
Figure 53	2D AFM image of 10 wt% ultrasonically mixed TiO <sub>2</sub> composite	37
Figure 54	Line analysis of 10 wt% ultrasonically mixed TiO <sub>2</sub> composite	37
Figure 55	3D AFM image of 10 wt% ultrasonically mixed TiO <sub>2</sub> composite	37
Figure 56	2D AFM image of 15 wt% ultrasonically mixed TiO <sub>2</sub> composite	37
Figure 57	Line analysis of 15 wt% ultrasonically mixed TiO <sub>2</sub> composite	38
Figure 58	3D AFM image of 15 wt% ultrasonically mixed TiO <sub>2</sub> composite	38
Figure 59	2D AFM image of 20 wt% ultrasonically mixed TiO <sub>2</sub> composite	38
Figure 60	Line analysis of 20 wt% ultrasonically mixed TiO <sub>2</sub> composite	38
Figure 61	3D AFM image of 20 wt% ultrasonically mixed TiO <sub>2</sub> composite	38
Figure 62	AFM image of 4 wt% showing the analysis of particle agglomerate size	39
Figure 63	Agglomerate size (Frequency distribution) as function of filler addition	40
Figure 64	Fracture surface image of pure epoxy	42
Figure 65	Fracture surface image of 2 wt% mech. Mixed sample	42
Figure 66	Fracture surface image of 4 wt% mech. Mixed sample	42
Figure 67	Fracture surface image of 6 wt% mech. Mixed sample	42
Figure 68	Fracture surface image of 8 wt% mech. Mixed sample	43
Figure 69	Fracture surface image of 10 wt% mech. Mixed sample	43
Figure 70	Fracture surface image of 15 wt% mech. Mixed sample	43
Figure 71	Fracture surface image of 20 wt% mech. Mixed sample	43
Figure 72	Fracture surface image of 15 wt% mech. Mixed sample at higher magnification	44
Figure 73	Fracture surface image of 20 wt% mech. Mixed sample at higher magnification	44
Figure 74	Fracture surface image of 2 wt% ultrasonically mixed sample	44
Figure 75	Fracture surface image of 4 wt% ultrasonically mixed sample	44
Figure 76	Fracture surface image of 6 wt% ultrasonically mixed sample	45
Figure 77	Fracture surface image of 8 wt% ultrasonically mixed sample	45
Figure 78	Fracture surface image of 8 wt% ultrasonically mixed sample at higher magnification	45
Figure 79	Fracture surface image of 10 wt% ultrasonically mixed sample	45



Figure 80	Fracture surface image of 10 wt% ultrasonically mixed sample at higher magnification	46
Figure 81	Fracture surface image of 15 wt% ultrasonically mixed sample	46
Figure 82	Fracture surface image of 15 wt% ultrasonically mixed sample at higher magnification	46
Figure 83	Fracture surface image of 20 wt% ultrasonically mixed sample	46
Figure 84	Fracture surface image of 20 wt% ultrasonically mixed sample at higher magnification	47
Figure 85	Fracture image of pure epoxy (Lap Shear Specimen)	47
Figure 86	Fracture image of 2 wt% ultrasonically mixed composite (Lap Shear Specimen)	47
Figure 87	Fracture image of 4 wt% ultrasonically mixed composite (Lap Shear Specimen)	47
Figure 88	Fracture image of 6 wt% ultrasonically mixed composite (Lap Shear Specimen)	48
Figure 89	Fracture image of 8 wt% ultrasonically mixed composite (Lap Shear Specimen)	48
Figure 90	Fracture image of 10 wt% ultrasonically mixed composite (Lap Shear Specimen)	48
Figure 91	Fracture image of 15 wt% ultrasonically mixed composite (Lap Shear Specimen)	48
Figure 92	Fracture image of 20 wt% ultrasonically mixed composite (Lap Shear Specimen)	49
Figure 93	Fracture image of 20 wt% ultrasonically mixed composite (Lap Shear Specimen) at edge	49
Figure 94	FTIR of TiO <sub>2</sub> nano particles	51
Figure 95	FTIR of pure polymer	51
Figure 96	FTIR of 2 wt% ultrasonic and mech. Mixed composite	52
Figure 97	FTIR of 4 wt% ultrasonic and mech. Mixed composite	52
Figure 98	FTIR of 6 wt% ultrasonic and mech. Mixed composite	52
Figure 99	FTIR of 8 wt% ultrasonic and mech. Mixed composite	53
Figure 100	FTIR of 10 wt% ultrasonic and mech. Mixed composite	53
Figure 101	FTIR of 15 wt% ultrasonic and mech. Mixed composite	53
Figure 102	FTIR of 20 wt% ultrasonic and mech. Mixed composite	54
Figure 103	FTIR plot of UV degraded pure polymer adhesive	55
Figure 104	FTIR plot of UV degraded 20 wt% TiO <sub>2</sub> ultrasonically mixed composite adhesive	55
Figure 105	Percentage degradation of strength as function of exposure days and amount of filler addition	56

## LIST OF TABLES

Table 1	Comparison of Joining Methods	5
Table 2	Mechanical Properties of epoxy/TiO <sub>2</sub> composite for different TiO <sub>2</sub> concentration	12
Table 3	Mechanical properties of epoxy/TiO <sub>2</sub> composite for different dispersing agent concentration	12
Table 4	Tensile strength for Mechanically mixed composites	27
Table 5	Tensile strength for Ultrasonically mixed composites	27
Table 6	Variation of Lap Shear Strength with filler amount	28
Table 7	IPDT results for Mechanically mixed composites	29
Table 8	IPDT results for ultrasonically mixed composites	29
Table 9	Percentage residual weight related to filler amount and temperature for mechanical mixing	30
Table 10	Percentage residual weight related to filler amount and temperature for ultrasonic mixing	30
Table 11	Details of Particle agglomerate size in 9 samples per wt% addition as per AFM analysis	40
Table 12	Comparison of pure and composite adhesive after UV degradation.	54
Table 13	Percentage decrease in strength of pure and composite adhesive as function of exposure time and amount of filler addition	56

# CHAPTER 1

# INTRODUCTION

---

The structural application of epoxy polymer largely suffers from its basic weaknesses of low stiffness and strength. These problems are often addressed to overcome by addition of inorganic particulate fillers such as SiO<sub>2</sub>, TiO<sub>2</sub>, ZrO<sub>2</sub>, Al<sub>2</sub>O<sub>3</sub> [1-4] and rubber [5-7] in the matrix. The size of these fillers are generally used in micrometer scale which enhances stiffness while degrades the fracture strain [8]. Such an adverse effect of addition of micron size particles can be overcome by adding nano-sized fillers in the matrix [8]. Nanoparticles provide extremely high specific surface area, which leads to interfacial interactions between the particles and the polymer matrix that primarily helps to achieve the new properties of the materials[9]. But the high specific area causes the nanoparticles to attract each other due to electrostatic Van der Waals forces and forming agglomerates with dimensions of several micrometers. To use the maximum benefit of high specific surface area of the nanoparticles they have to be homogeneously dispersed in the polymer matrix. It may happen due to increase of effective interfacial contact between the fillers and the matrix and wide spread interaction of the nano particles with the basic molecular arrangement of the matrix. A well bonded interface allows a smooth transfer of applied load from the matrix to nanoparticles. Good dispersion of particles also results in a more uniform stress distribution and minimizes stress - concentration centres in the matrix which enhances the general strength and modulus of the composites [10].

A large amount of work has been reported on polymer composites having filling of TiO<sub>2</sub> particles showing their influence primarily on the elastic modulus, elongation at break point and toughness of the composite. In some work incorporation of TiO<sub>2</sub> particles of the order of 4 wt% in polymer gives optimum properties of the composite while in some other study the tensile strength and scratch resistance of polymer composite have been found to be maximum at 10 wt% of micron sized TiO<sub>2</sub> particles [8]. Gradually, nano particles are fast replacing micron sized particles as fillers to get better properties. Considerable amount of work has been done on wear properties of TiO<sub>2</sub> nanoparticle filled epoxy adhesives. The specific wear rate of a neat epoxy was reduced by about 4 times by the incorporation of 300 nm TiO<sub>2</sub> (4 vol. %) particles [13]. Epoxy nanocomposite containing graphite powder (7 vol.

%), TiO<sub>2</sub> (4 vol. %) was additionally filled with short Carbon fibres (SCF), aramid fibres and Poly-tetrafluoroethylene (PTFE) particles and tested for low amplitude oscillating wear resistance which showed poor results for 2-4 vol. % PTFE filled SCF nanocomposite [14]. Toughening effects of TiO<sub>2</sub> nanoparticle filled epoxy adhesive has been studied which has shown improvement in plane strain fracture toughness, tensile strength, elastic modulus and maximum sustained strain at lower TiO<sub>2</sub> additions[9]. No significant work has been reported in the fields of thermal properties, lap shear strength and ultrasonic degradation for TiO<sub>2</sub> particles filled polymer nano composites. Afore mentioned works prompted us to explore the possibility of enhancement of various properties of structural epoxy adhesive by incorporating nano sized TiO<sub>2</sub> as filler material and in addition to obtain mechanical properties at both lower and higher TiO<sub>2</sub> nano particles addition.

The primary objective of the present work was to synthesize inorganic nanoparticle filled epoxy adhesive having largely homogenous dispersion of different amounts of TiO<sub>2</sub> nano-particles and to study their influence on mechanical and thermal properties of the matrix. The fracture behaviour of the with / without particle filled epoxy adhesive has been studied under Scanning Electron Microscope. Furthermore, UV degradation of the pure and the composite epoxy adhesives has been studied and compared. Effort has also been made to study the lap shear strength of Metallic joints of the pure and composite epoxy adhesives.

## CHAPTER 2 LITERATURE SURVEY

---

**2.1 ADHESION:-** Adhesion is the phenomenon which allows two objects to retain surface contact non-magnetically. Most theories of adhesion can be expressed in terms of electrical attractions. Essentially, certain minute locations on one surface possess or acquire positive or negative electrical charges which then align themselves adjacent to an oppositely charged location on the other surface.

There are several methods to join metals and materials. They are: -

- a) Welding
- b) Brazing
- c) Soldering
- d) Mechanical Joints like riveting, bolting, etc.
- e) Adhesive Bonding

### 2.1.1 ADVANTAGES OF ADHESIVE BONDING

#### 2.1.1.1 Fabrication of Smooth Exterior Surfaces

Adhesive remains in-between joined surfaces and thus it eliminates the need for surface finishing, such as that required to grind down rivet heads, etc. Smooth exterior surfaces imply less drag and more efficient gaseous and fluid flow patterns over or around aerodynamic faces. The absence of protruding bolt or rivet heads also signifies that there are no concentrated stress sites in the attachment area. Forces are dispersed over the entire assembly face.

#### 2.1.1.2 Protection Against Shock and Vibration Failure

The elastomeric nature of most adhesives results in an energy absorbing response to impact and fatigue forces. The ability of adhesively bonded structures to withstand significantly

higher sonic fatigue levels than mechanically fastened counterpart in both subsonic and supersonic aircraft applications is an illustration of this property. Transmission of sound is drastically reduced by passing through an adhesive interlayer. Most polymeric adhesive systems are poor thermal conductors, they act to soak up stresses induced by thermal cycling, particularly in metallic structures. To prevent vibrational loosening, anaerobic adhesives are used as interference fit materials between threaded fasteners and the structures into which they are inserted. The automotive and farm implement industries use adhesives to great advantage in this type of application.

#### **2.1.1.3 Use of Light Gauge Materials**

Stresses applied to a bonded structure are spread over a large area compared to stresses directed to and through local sites, such as bolts of a linear assembly. To compensate for strength reduction due to these stresses at local sites (holes for bolts, rivets), generally the parts are overdesigned in strength (made thicker and heavier). Sometimes top layers of any additional material are incorporated by an adhesive, to achieve required properties such as surface reflectivity, conductivity, insulation, corrosion resistance, abrasion resistance, etc.

#### **2.1.1.4 Joining of Dissimilar Materials**

Prevents galvanic corrosion. Also adhesives have good electrical insulation and poor thermal conductivity. Stresses caused by rapid thermal cycles are reduced by slow heat transfer through the adhesive. Dimensional distortion of the assembly, caused by different coefficients of thermal expansion, is reduced by the heat-sink action of the adhesive. Bonded assemblies derive their prime strength from the chemical interlocking of the adhesive with a substrate, the relative modulus (stiffness) and chemical nature (metal, plastic, glass, ceramic, etc.) of the attached surfaces do not have to be as closely matched as those of most mechanically attached components.

### 2.1.1.5 Simplified Joining of Contoured or Delicate Parts

Flat assemblies normally do not present mating problems even for mechanical fastening. Curved or multi-contoured surfaces present an entirely different situation. Surface loading of bonded assemblies transfers stress through a continuous, gap-filling, substrate membrane, which is connected to next-in-line components or faces. This fact allows the relaxation of fit tolerances. The reduced fit, or mating-gap tolerance requirement can often result in lower component preparation costs and can simplify jig or fixturing setups.

### 2.1.1.6 Reduced Cost of Manufacture and Assembly

Frequently, a mechanically fastened assembly required secondary operations, such as sealing or filling gaps between fastener sites. E.g. water tanks, storage bins. Primary mechanical strength or holding power considerations do not totally fill the functional requirements of the assembly. Adhesive bonding of such assemblies satisfies the requirements for both mechanical strength and end use.

**TABLE 1 COMPARISON OF JOINING METHODS**

TOPIC OF COMPARISON	RIVETING	WELDING	BRAZING	ADHESIVE BONDING
Preliminary machining	P	E	P	E
With thin metals	P	P	F	E
Limits on metal combinations	F	P	P	E
Surface Preparation	E	G	F	P
Tooling	E	F	F	F
Need for access to joint	P	P	E	E
Heat requirements	E	P	P	F-G
Stress Distribution	P	F-G	E	E
Sealing Function	P	F	E	G
Rate of strength development	E	E	E	P

Distortion of assembly	F	P	F	E
Final machining	G-E	F	E	E
Final Heat treatment	E	F	F	E
Solvent resistance	E	E	E	F
Effect of temperature	E	E	E	P
Ease of repair	G	P	P	F
Level of skill required	E	G	E	E

E = Excellent G = Good F = Fair P = Poor

**Polymer** is the material which forms the bulk of most adhesive films. It is a plastic like material. It is made by the repetitive joining of many small chemical units (molecules). These chemical units are held together by covalent bonds[2]. Most of the bulk properties of an adhesive material, such as heat resistance and tensile strength, are primarily due to the nature of the polymer used in the adhesive. The length of polymer chain is specified by the number of repeating units in two chains. This is termed as degree of polymerization. The molecular weight of polymer is obtained by the product of the molecular weight of repeating unit and the degree of polymerization.

## 2.2 EPOXY RESIN

Epoxy is a thermosetting epoxide polymer that cures (polymerizes and cross links) when mixed with a catalyzing agent or "hardener". Epoxy is a copolymer, i.e. it is formed from two different chemicals. These are referred to as "resin" and "hardener". Most common epoxy resins are produced from a reaction between epichlorohydrin and bisphenol-A.



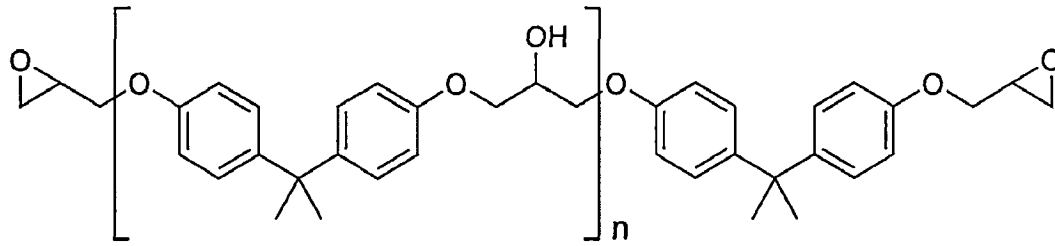


**Figure 1:- Structure of unmodified epoxy prepolymer. “n” denotes the number of polymerized subunits and is in the range of 0 to 25**

The applications for epoxy based materials are extensive and include coatings, adhesives and composite materials such as those using carbon fiber and fiberglass reinforcements. The chemistry of epoxies and the range of commercially available variations allows cure polymers to be produced with a very broad range of properties. In general, epoxies are known for their excellent adhesion, chemical and heat resistance, good to excellent mechanical properties and very good electrical insulating properties, but almost any property can be modified (for example silver-filled epoxies with good electrical conductivity are available, although epoxies are typically electrically insulating).<sup>(3)</sup>

Epoxy adhesives are a major part of the class of adhesives called "structural adhesives" or "engineering adhesives" (which also includes polyurethane, acrylic, cyanoacrylate, and other chemistries.) These high performance adhesives are used in the construction of aircraft, automobiles, bicycles, golf clubs, skis, snow boards, and other applications where high strength bonds are required. Epoxy adhesives can be developed that meet almost any application. They are exceptional adhesives for wood, metal, glass, stone, and some plastics. They can be made flexible or rigid, transparent or opaque/colored, fast setting or extremely slow. Epoxy adhesives are almost unmatched in heat and chemical resistance among common adhesives. The strength of epoxy adhesives is degraded above 177°C. In general, epoxy adhesives cured with heat will be more heat- and chemical-resistant than when cured at room temperature.<sup>(3)</sup>

The two component epoxy paste adhesive which will be used in the dissertation work is a commercially available adhesive system ARALDITE 2011 (AW 106/HV 953U)

## **2.3 ARALDITE 2011[23]**

Araldite 2011 is a multipurpose, two component, room temperature curing, paste adhesive of high strength and toughness. It is suitable for bonding a wide variety of metals, ceramics, glass, rubber, rigid plastics and most other materials common in use. It is a versatile adhesive for the craftsman as well as most industrial applications.

### **2.3.1 KEY PROPERTIES:-**

1. High shear and peel strength
2. Tough and Resilient
3. Good Resistance to dynamic loading
4. Bonds a variety of materials in common use

### **2.3.2 PROCESSING:-**

**A) Pre-Treatment:-** The strength and durability of bonded joint are dependent on proper treatment of surfaces to be bonded. Joint surfaces should be cleaned with good degreasing agent like acetone or other proprietary degreasing agents in order to remove all traces of oil, grease and dust. Low grade alcohol, gasoline or paint thinners should never be used. The strongest and most durable joints are obtained by either mechanically abrading or chemically etching the degreased surface. Abrading should be followed by a second degreasing treatment. Resin and hardener are mixed in ratio 100:80 by weight. They are blended until they form a homogenous mixture.

**B) Application of Adhesive:-** The resin/hardener mix is applied with a spatula, to the pretreated and dry joint surfaces. A layer of adhesive 0.05 to 0.10 mm thick will normally impart the greatest lap shear strength to the joint. The joint components should be assembled and clamped as soon as the adhesive has been applied. An even contact pressure throughout the joint area will ensure optimum cure.

## 2.4 TITANIUM DIOXIDE NANO PARTICLES

Titanium dioxide (TiO<sub>2</sub>) nano materials are used in a wide range of applications such as (photo)catalysis, separations, sensor devices, paints, and dye-sensitized solar cells. The material properties of TiO<sub>2</sub> nanoparticles are a function of the crystal structure, nanoparticle size, and morphology. TiO<sub>2</sub> exists in three main phases: anatase, brookite and rutile[2]. Titanium dioxide was first industrially introduced to replace toxic lead oxide as a white paint pigment in early 1900's. Titanium dioxide is corrosion protective, can be dispersed easily as well as absorbs incident UV and thus protects paint from direct photochemical of organic binder, making it suitable for paint industry. Water is easily absorbed at the surface of TiO<sub>2</sub>. It has chemically active surface which is capable of absorbing, dissociating or reacting with wide variety of inorganic and organic molecules.

## 2.5 PARTICULATE FILLED POLYMER COMPOSITE

Composite material having particles of substances such as metal, glass or ceramics as fillers and they are typically suspended in a reinforcing matrix (polymer) pattern throughout the material[6]. Highly cross linked thermosetting polymers like epoxy resins are an important class of synthetic materials. Due to high density of cross linking, properties including high glass transition temperatures, high modulus and specific strength, high creep resistance, good dimensional stability at elevated temperature, and good solvent resistance. They are extensively used as adhesives, electronic substrates and packaging, tooling compounds and most importantly as matrix materials for reinforcing composites. Due to high degree of cross linking these polymers are inherently brittle and have poor resistance to crack initiation and propagation. The lack of toughness severely impacts the performance of these thermosets in most applications[7]. To improve the toughness of thermosetting resins is one of the topics of current research. Additions of micron and nano size soft (elastomeric or thermoplastic) or rigid particles (glass or ceramic) in the polymer matrix have been carried out to improve various properties. Addition of soft particles in matrix improves the toughness moderately but the elastic modulus and high temperature performance are compromised. While studies

show that incorporation of high modulus ceramic particles generally improve the elastic modulus and glass transition temperature with, moderate increase in fracture toughness [7].

## 2.6 WORK REPORTED IN LITERATURE ON TiO<sub>2</sub> POLYMER COMPOSITE

A. A. Wazzan, H. A. Al-Turaif, A. F. Abdelkar [20] found the effect of TiO<sub>2</sub> addition to epoxy by mechanical mixing and studied mechanical properties of composite. Matrix was prepared using a two component system, DER 331 (it is undiluted diglycidyl ether of Bisphenol A) used as resin and Ethacure 100 used as the curing agent. They were mixed in the ratio 100 parts by weight of epoxy to 23.91 parts by weight of hardener. Reinforcing agent is Rutile Titanium dioxide of approx. size 190 nm. They used a moderate speed paddle mixer (mechanical mixing) to disperse the particles in epoxy system, mixing time varied from 10 – 30 mins., depending on amount of TiO<sub>2</sub> particles added. The mixture was degassed for 30 mins. at 80°C and -700 bar pressure. Now hardener was carefully added and again degassed for 10 mins. Curing was done in nitrogen atmosphere for 5 hrs at 110°C, followed by another 5 hrs at 185°C.

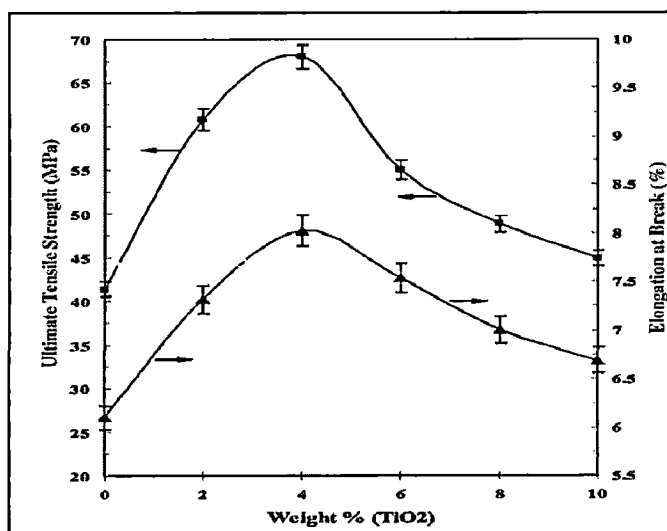


Figure 2:- Ultimate Tensile Strength and Elongation at Break as a function of weight fraction of submicron size titanium dioxide particles.

XPS was used to confirm that TiO<sub>2</sub> are uniformly dispersed within the epoxy matrix. Tensile testing was carried out on dumbbell shaped samples (ASTM D-638-91, Type I) using UTM at 23°C at extension rate of 0.5 mm/min. Impact testing was also carried out using charpy impact testing machine and the data was analysed by ASTM standard D-5045-95. Similar results are obtained for Toughness, Young's Modulus, Critical Stress Intensity Factor and

Critical Strain Energy release rate i.e. all these properties are found to be maximum at 4 wt% of titanium dioxide addition as filler as seen in the above figure. They have attributed the increase in mechanical properties of composite to the formation of micro-voids, which absorb some of the deformation work during the application of mechanical stress.

C.B. Ng, L.S. Schadler and R.W. Siegal found the effect of TiO<sub>2</sub> reinforcement on Strain to failure and Scratch Indentation. They compared the properties of nano and micron size particle addition to epoxy[22].

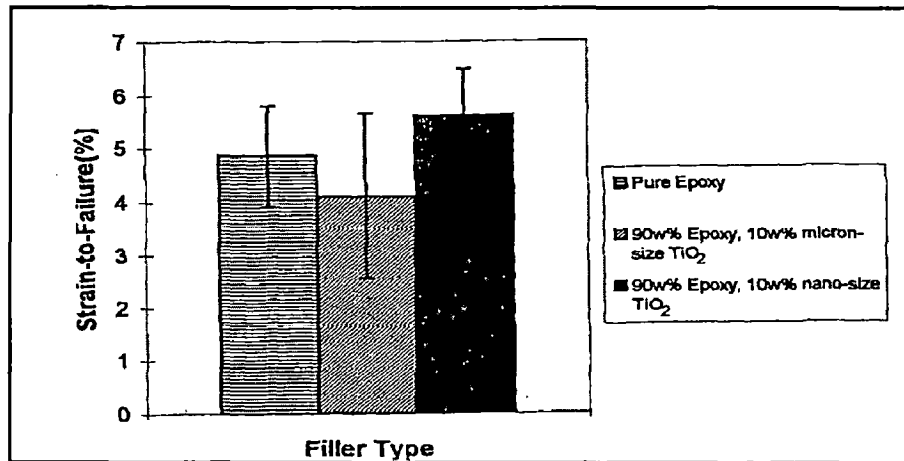


Figure 3:- Effect of different size of TiO<sub>2</sub> fillers on the strain to failure of composite

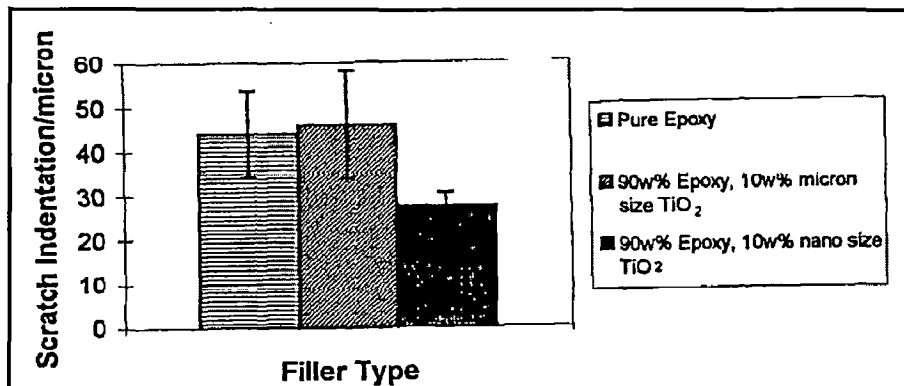


Fig. 4:- Effect of different size of TiO<sub>2</sub> fillers on the scratch indentation of composite

K.S. Huang, J.W. Chen and coworkers found the properties of epoxy TiO<sub>2</sub> composites when the dispersion agent and amount of TiO<sub>2</sub> is varied[34]. Epoxy / TiO<sub>2</sub> composites were prepared by solution mixing method in which epoxy resin and nano TiO<sub>2</sub> liquid were mixed in presence of methyl isobutyl ketone. Mechanical properties are found to improve with

addition of TiO<sub>2</sub> but properties degrade if the amount of particles is more than 3%. The decrease in properties has been attributed to two factors. One is, due to increase in nano sized particles, excessive proximity among particles and bigger fractures from tiny cracks. Second is, increase in particles make it difficult to disperse them properly and chances for agglomeration are higher.

**TABLE 3. Mechanical properties of Epoxy/TiO<sub>2</sub> composites<sup>a</sup> on different TiO<sub>2</sub> liquid concentrations.**

TiO <sub>2</sub> liquid conc. (%)	Properties			
	Stretch strength (kgf/cm <sup>2</sup> )	Compression strength (kgf/cm <sup>2</sup> )	Flex strength (kgf/cm <sup>2</sup> )	Impact strength (kgf-cm)
0				
1.5	81.27	557.89	6.02	2.38
3.0	86.98	584.60	7.04	2.91
5.0	86.47	580.32	6.83	2.82
7.0	85.25	564.11	6.32	2.39
10.0	80.15	433.48	5.10	1.94

<sup>a</sup>Concentration of dispersing agent is 3.6%.

**Table 2:- Mechanical Properties of epoxy/TiO<sub>2</sub> composite for different TiO<sub>2</sub> concentration**

Dispersing conc. (%)	Properties			
	Stretch strength (kgf/cm <sup>2</sup> )	Compression strength (kgf/cm <sup>2</sup> )	Flex strength (kgf/cm <sup>2</sup> )	Impact strength (kgf-cm)
0				
1.2	61.90	532.90	6.63	1.88
2.4	64.14	582.16	6.93	2.30
3.6	86.98	584.60	7.04	2.91
5.0	109.93	588.07	7.75	3.21

<sup>a</sup>Concentration of TiO<sub>2</sub> is 3%.

**Table 3:- Mechanical properties of epoxy/TiO<sub>2</sub> composite for different dispersing agent concentration**

Pablo Carballeira and Frank Hauptert [9] added upto 10 volume percent TiO<sub>2</sub> nano particles to epoxy resin using a torus mill device to homogenously disperse the former in latter. It was shown that addition of TiO<sub>2</sub> nanoparticles in low volume concentrations to the epoxy resin could simultaneously improve the stiffness, toughness, maximum sustained strain, and resistance to crack propagation of the neat resin. The mechanical properties depend strongly on the volume fraction of fillers incorporated to the epoxy. The improved properties of the composites can be ascribed to the presence of the TiO<sub>2</sub> nanoparticles in the

resin, which leads to energy dissipation through different mechanisms such as crack pinning at particles, crack deflection at particle agglomerates or shear yielding of the matrix.

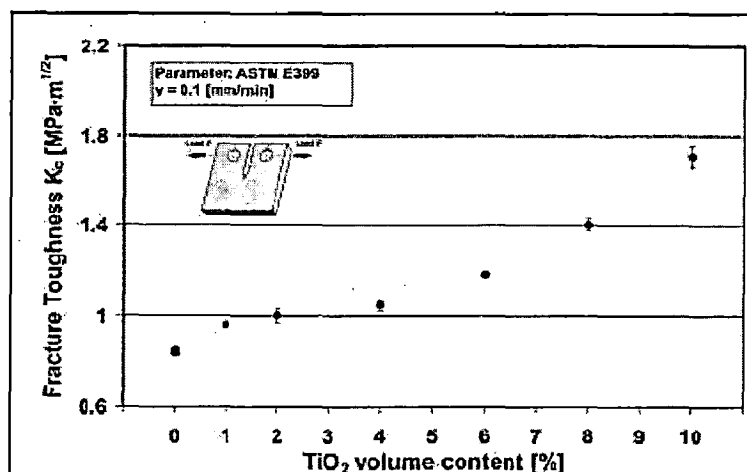


Figure 5:- Static Fracture toughness K<sub>IC</sub> of composite as function of filler amount

Yuan Qing Li and coworkers [18] have found the potential of TiO<sub>2</sub>-Silica filled polymer nano composite in UV LED lamps. It was reported that the life of UV LED lamp encapsulated with Silica-Titania-Silica epoxy composite was increased by 54% compared to pure epoxy encapsulated UV LED lamp and an increase of 33% was reported in lifetime of UV LED lamp encapsulated with Silica-Titania epoxy composite. Manwar Hussain and coworkers [34] found the fracture toughness for epoxy TiO<sub>2</sub> system. Fracture toughness for an epoxy-TiO<sub>2</sub> composite system was evaluated at room and liquid N, temperature in which both the volume and the particle size of dispersoid have been changed. Tetra functional epoxy resin, 1,2-cyclo-hexanedicarboxylic anhydride are used as materials, with nano (20 nm) and micron (1 micron) size fillers. Epoxy and particles were mixed with ball mill technique, dried, hardener was mixed, placed in vacuum, and cured at 80°C for 2 hrs and post curing at 180°C for 2 hrs. The fracture toughness test was conducted and the results are shown below.

High Toughness value of micron size particles dispersed epoxy was suggested due to step wise crack jump releasing large amount of excess energy which is dissipated as crack branching or plastic deformation. As per the studies of Prof. P.K. Ghosh and S.K. Nukala, [26] the properties of epoxy adhesive can be significantly improved by addition of nano zirconia particles. The optimum wt.% of zirconia as reinforcement was found and its metallic joint (Aluminum strips mechanically treated) Lap shear strength was also

studied[15]. The LSS was found as a function of bond line thickness and it was found that at 0.1 mm bond line

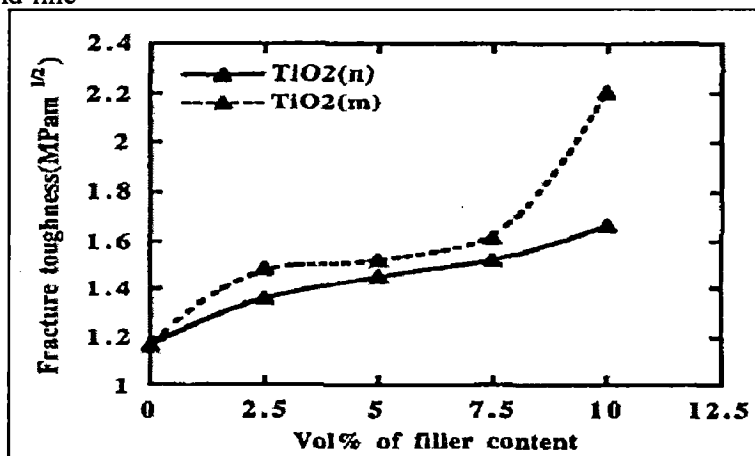


Fig. 6:- Fracture toughness as a function of filler content

thickness maximum strength can be obtained. Mechanical interlocking of composite adhesive in the metallic joint by roughening the surface of Aluminum gave good strength.

## 2.7 EFFECT OF PARTICLE SIZE, PARTICLE/MATRIX INTERFACE ADHESION AND PARTICLE LOADING ON MECHANICAL PROPERTIES OF PARTICULATE POLYMER COMPOSITES [25]

### 2.7.1 Young's Modulus:-

#### 2.7.1.1 EFFECT OF PARTICLE SIZE AND AMOUNT

No significant effect of particle size, if particle size is greater than 30 nm. Below particle size of 30 nm, Young's modulus increases with decrease in size of particle. Young's Modulus is improved with the increase in amount of particles as they have much higher Young's modulus than matrix.

#### 2.7.1.2 EFFECT OF PARTICLE/MATRIX INTERFACIAL ADHESION



Modulus is independent of interfacial adhesion. Since young's modulus is measured at relatively low deformation, there is insufficient dilation to cause interface separation. Thus it is easy to understand that adhesion strength does not noticeably affect the elastic modulus.

### 2.7.1.3 EFFECT OF PARTICLE LOADING

Addition of rigid particles to polymer matrix can easily improve the modulus since the rigidity of inorganic fillers is generally much higher than that of organic polymers. Composite modulus continuously increases with increase in particle loading.

### 2.7.1.4 THEORIES FOR ELASTIC MODULUS:-

Nano particles restrict polymeric molecular diffusion. This occurs because of an effective attraction potential between segments of chain and repulsive potential that the polymer is subjected to when it is close to solid particles. The degree of particle restriction depends on properties of filler and matrix. This effect of interphase enhances the composite modulus.

The Rule of Mixtures for composites has been modified to get the young's modulus of composite for small fraction of particulate addition.

$$E_c = X_p \cdot E_p \cdot V_p + E_m \cdot (1 - V_p)$$

Where,  $X_p$  = Particle strengthening factor, lies between 0 and 1

$E_p$  = Young's modulus of reinforcement particles

$E_m$  = Young's modulus of matrix

$V_p$  = Volume fraction of reinforcement particles

$E_c$  = Young's modulus of Composite

For higher volume fraction of reinforcing particles, Mori – Tanaka Micromechanics method can be used. It assumes each inclusion in the infinite pristine matrix loaded by an effective stress that equals the average stress over the matrix. The effective modulus of particulate dispersed composite is given by:-

$$E_c = 9 \cdot K_c \cdot G_c / (3K_c + G_c)$$

Where,  $K_c$  = bulk modulus of composite

$G_c$  = shear modulus of composite

$$K_c = K_m + \{V_p.K_m.(K_p - K_m)\} / \{K_m + B_2(1 - V_p).(K_p - K_m)\}$$

$$G_c = G_m + \{V_p.G_m.(G_p - G_m)\} / \{G_m + B_1(1 - V_p).(G_p - G_m)\}$$

The conventions for symbols are the same, “m” for matrix and “p” for particles

## 2.7.2 Strength

### 2.7.2.1 EFFECT OF PARTICLE SIZE AND AMOUNT

Strength is the maximum stress that the material can sustain under uniaxial tensile loading. Strength increases with decrease in particle size. Various studies have shown that the effect of particle amount is uncertain on strength, it depends on the composite in study.

### 2.7.2.2 EFFECT OF PARTICLE/MATRIX INTERFACE ADHESION

Strength and toughness are very much dependent on adhesion quality. Work of adhesion can be determined from contact angle measurement or by contact mechanics. Effective stress transfer is an important factor which contributes to strength of two phase composite material. For poorly bonded particles, the stress transfer at particle/matrix interface is inefficient as discontinuity in the form of debonding exists because of non-adherence of particle to the polymer. Thus, particle cannot carry any load and composite strength decreases with increase particle loading. However, for well bonded particles, composite strength increases with increase in particle loading specially for nanoparticles having high surface area.

### 2.7.2.3 THEORIES OF STRENGTH

Ultimate strength of the composite will depend on the weakest fracture path throughout the material. Hard particles affect strength in two ways:-

1. Weakening effect, due to stress concentration they cause due to their presence in the matrix.
2. Reinforcing effect since they may serve as barrier to crack growth and propagation.

In some cases the weakening effect is predominant and thus the composite strength is lower than the matrix; and in other cases, the reinforcing effect is more significant and then the composite will have strength higher than the matrix. Prediction of strength of composite is difficult. The difficulty arises because the strength of composite is determined by the fracture behaviors which are associated with the extreme values of such parameters as interface adhesion, stress concentration and defect size/spatial distribution. Thus the load bearing capacity of a particulate composite depends on the strength of the weakest path throughout the microstructure rather than the statistically averaged values of microstructure parameters.

### 2.7.3 Fracture Toughness

#### *2.7.3.1 EFFECT OF PARTICLE SIZE AND AMOUNT*

For filler as micron size particles, the fracture toughness increases with increase in particle size, but it is not true for sub-micron and nano sized particles. Fracture toughness values reaches a maximum and at some particular volume fraction and decreases on both sides of it. Effect of particles size, shape and amount is closely linked with particle/matrix interfacial adhesion as the mechanism of failure is different for different composites.

#### *2.7.3.2 EFFECT OF PARTICLE/MATRIX INTERFACIAL ADHESION*

In thermosetting polymers, crack growth is dominated by matrix failure and particle breakage. Thus, interfacial bonding is of less importance and efforts made to improve the interfacial adhesion are not much effective to increase the toughness. In thermosets, Fracture toughness value is generally higher than that of neat epoxy but not as high as in case of thermoplastics having particulate filler in it.

#### *2.7.3.3 THEORIES FOR FRACTURE TOUGHNESS*

There are a range of possible toughening mechanisms proposed for various composite systems, such as:-

- a) Crack front bowing (or crack pinning)
- b) Crack tip blunting
- c) Particle matrix interface debonding
- d) Crack deflection by hard particles
- e) Breaking of particles

The mechanisms of crack interaction with a second phase dispersion have been studied by different researchers, generally two different types of fracture surfaces are observed. One type included surface steps associated with each particle encountered by the moving crack front. They are a characteristic feature of the interaction of a crack with inhomogeneities, such as voids and second phase particles. This type of surface was only observed for composites containing dispersed phase volume fractions smaller than that resulting in peak toughness. The second type of surface appeared similar to that of polycrystalline materials. Such surfaces were found for composites with volume fractions larger than that yielding peak toughness. A combination of both types of fracture surfaces was observed for composites with peak toughness. In general, for large interparticle spacing, a surface containing steps was observed. For small interparticle spacing, the surface appeared polycrystalline. During fracture, a moving crack is momentarily pinned at positions of inhomogeneities within the brittle matrix. This interaction leads to crack front bowing, thus increasing its total length when the particle spacing decreases and the line tension rises. However, a maximum is reached inferring that the dispersed particles become too closely spaced to interact effectively with the crack front. Smaller particles are less effective as anchors than larger particles. Therefore, the fracture toughness is higher for the composite containing larger particles. Particle/matrix interface adhesion was found to affect both the crack growth behavior and the appearance of the fracture surface of glass bead filled epoxy micro-composites. The main toughening mechanism is crack pinning. For poorly bonded particles, the crack is attracted to the equators of the particles and moves around the particles. The fracture surface consists of hemispherical holes and top surfaces of debonded particles. For well-bonded particles, the crack is attracted to the poles of the particles. The crack then propagates through the matrix above or below the particles leaving a layer of epoxy resin covering them. Weak interfacial adhesion between rigid particles and matrix makes crack pinning less effective because debonded particles are ineffective as pinning sites.

## 2.8 ULTRASONIC CAVITATION METHOD [28]

Cavitation is formation of bubbles / cavities in liquid medium. During the rarefaction portion of the cycle, when the pressure in the wave is below ambient, gas pockets may form and expand with the impressed field. These gases may be of two types: (1) those that have been dissolved or trapped in minute bubbles in the liquid or on surfaces in contact with the liquid and (2) vapors of the liquid itself. The first of these produces gaseous cavitation, low intensity while second type is called vaporous cavitation, fairly high intensity. If the pressure within the cavity is lower than the vapor pressure of the liquid during the expansion phase, the bubble is a result of fragmentation due to the tensile stress imposed by the ultrasonic wave being equal to the tensile strength of the liquid. This type of cavitation is very intense. The tensile strength of the liquid imposes an upper limit on the amplitude of the stress of the ultrasonic wave used to produce cavitation. It is unlikely that the true strength of liquid is ever reached in practice because most liquids contain nuclei about which cavitation bubbles originate. These nuclei may consist of dispersed dust particles, prominences on immersed surfaces, or minute gas bubbles. High localized stresses are developed during the formation and subsequent collapse of cavitation bubbles. Some effects produced in the presence of cavitation include increased chemical activity, erosion of surfaces, rupture or fragmentation of suspended particles, emulsification of liquid mixtures, and dispersion of small particles in the liquid. The onset of cavitation occurs at intensities, or cavitation thresholds, that depend upon such factors as the sizes of nuclei, ambient pressure, amount of dissolved gases, vapor pressure, viscosity, surface tension, the frequency and duration of the ultrasonic energy. When cavitation occurs, it not only dissipates the ultrasonic energy, but it impedes transmission of sound past it. To cause effective expansion and violent collapse of cavitation bubbles, the bubble must be capable of expanding with the rarefaction part of the cycle of the impressed field and of collapsing before the total pressure reaches its minimum value.

## CHAPTER 3 EXPERIMENTAL WORK

### 3.1 CHARACTERIZATION OF TITANIUM DIOXIDE PARTICLES

The titanium dioxide particles were purchased from American Elements Los Angeles, CA, USA. Characterization of titanium dioxide particles included the XRD to find the phase of titanium dioxide and TEM image to find the particle shape and size. As per the XRD plot (figure 7), it was found that the TiO<sub>2</sub> powder is having Anatase phase. The TEM image (figure 8) shows that the TiO<sub>2</sub> particles are having size in nanometer range,  $25 \pm 5$  nm and the shape is square with rounded edges.

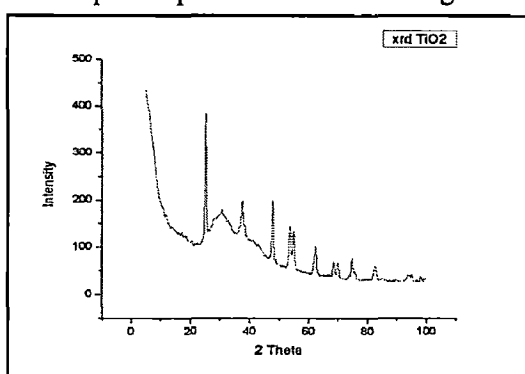


Fig. 7:- XRD plot of TiO<sub>2</sub> particles

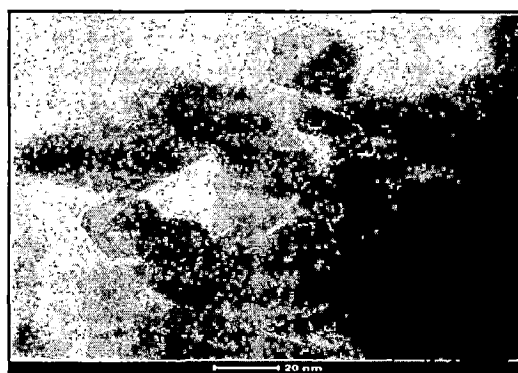


Fig. 8:- TEM image of TiO<sub>2</sub> particles

### 3.2 Composite Adhesive Sample Preparation (Mechanical Mixing & Ultrasonic Mixing)

#### 3.2.1 Sample preparation for tensile testing

The epoxy and hardener were dried for 30 min at 60°C. The epoxy resin (AW 106) and hardener (HV 953 U) are mixed as (100 : 80). TiO<sub>2</sub> particles are taken as 2, 4, 6, 8, 10, 15, 20 wt.% of epoxy resin. Say for example we are making a 2wt.% TiO<sub>2</sub> composite adhesive sample. So the amount of epoxy resin will be 2.78 g, hardener will be 2.22 g and the amount of TiO<sub>2</sub> particles will be  $0.02 \times 2.78 = 0.0556$  g. Similar calculations for other wt.% of TiO<sub>2</sub>. Take required amount of epoxy resin and TiO<sub>2</sub> particles in a glass beaker cleaned with acetone. Take required amount of hardener in other glass beaker cleaned with acetone. Mechanically mix the epoxy and TiO<sub>2</sub> particles until we get a homogenous mixture (mixing

can be agitator or hand mixing). In our case it is hand mixing till we find a homogenous mixture of nano particles in the epoxy.

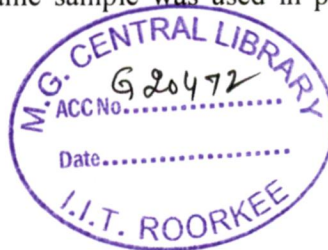
For Ultrasonic mixing, the mixture of TiO<sub>2</sub> particles and epoxy in required amount, were taken and mixed with Ethyl Methyl Ketone as a solvent. After proper mixing in the solvent, the mixture was mixed using Ultrasonic Vibracell with the following parameters. Amplitude 55%, on time 20 sec, off time 50 sec., time 4 hrs (on time) and temperature is kept below 30°C. These parameters are optimized by prior experiments. Add hardener in homogenous mixture and again stir till we get uniform mixture. Curing starts in the glass beaker. Place the mixture in vacuum desiccator for 15 to 20 min depending on the removal of entrapped air. Take care that during the whole manufacturing procedure, temperature of the system should not go above 30°C. Mould of glass is cut in required dimensions as per ASTM D 638-08. The mixture is taken out from vacuum and carefully poured (to avoid air entrapment) in the mould, treated with releasing agent. Curing is done at 40°C for 16 hours in hot air oven. The samples were polished with 1/0 to 4/0 samples along the gauge length to avoid any type of stress risers before performing the tensile test.

### 3.2.2 Sample preparation for Atomic Force Microscopy (AFM)

Petri dish of glass is cleaned with acetone and releasing agent is applied on it. The mixture is taken out of vacuum, taken on a spatula and is gently sprayed on the Petri dish. Curing is done at 40°C for 16 hours in oven. The cured composite adhesive is stripped off from the Petri dish and the smoother side of sample is taken for AFM

### 3.2.3 Sample Preparation for DTA/TGA and FTIR

The sample prepared for AFM were taken and small pieces are cut out of it. Generally small size of square/rectangular samples are taken. The samples were cleaned with acetone and used for DTA/TGA analysis. The same sample was used in powder form using abrasive method in order to get FTIR samples.



### 3.2.4 Sample Preparation for Lap Shear Test

Aluminum plates of dimensions 200 mm x 2 mm x 15 mm (length x thickness x width) were used for Lap Shear Test. The plates were degreased and polished along the width direction using coarse sand paper to get mechanical bonding of adhesive with the plates. The polished plates were cleaned subsequently with water and acetone. The bond dimensions are 1.5 mm x 15 mm x 12.5 mm (thickness x width x length)

### 3.3 Tensile Testing[16]

It is the standard for tensile testing of plastics.

As per this standard the sample should have dimensions as follows:-

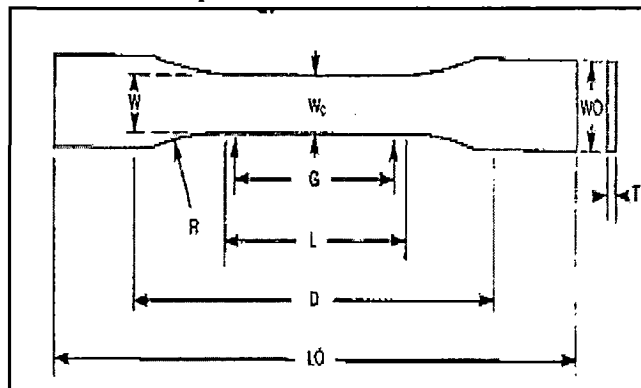


Figure 9:- Drawing of ASTM D 638-08 tensile test specimen

- ✓ w-width of narrow section 3.18 +/- 0.5 mm
- ✓ L-length of narrow section 9.53 +/- 0.5 mm
- ✓ T-thickness 4 mm or under
- ✓ W0-width overall 9.53 +/- 3.18 mm
- ✓ L0-length overall 63.5 mm
- ✓ G-gauge length 7.62 +/- 0.25 mm
- ✓ D-distance between grip 25.4 +/- 5 mm
- ✓ R-radius of fillet 12.7 +/- 1 mm

✓ The conditions of testing are listed below:-

- ✓ Temperature 23 +/- 2 °C
- ✓ Humidity 50 +/- 5 %
- ✓ Speed of Testing 1 mm/min +/- 25%

The tensile test was carried out for minimum three to maximum five samples which were free of defects. The defects mainly include a deformed shape or presence of air bubble or



any sort or in-homogeneity in the material. The average results were plotted as the variation of stress with respect to wt.% titanium dioxide addition. The test was carried out for both mechanically mixed and ultrasonically mixed composites.

### 3.4 LAP SHEAR TESTING[18]

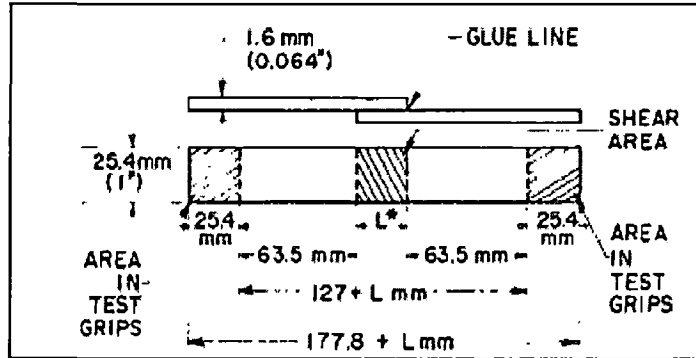


Fig 10. Details of lap shear specimen

Lap shear strength was determined according to ASTM D 1002 and was carried out on the same machine. The dimensions of test sample are given in Fig. and the crosshead speed was 1.3 mm/min. For each composition, the average result from at least five samples was determined.

### 3.5 STUDY OF THERMAL PROPERTIES

DTA/TGA test was performed for at least three samples of each composition. The samples for test were prepared as small pieces of roughly 3 mm x 3 mm from the thin film prepared on petry dish. The test was carried out on the Thermal Analyser (Perkin-Elmer, Pyris Diamond) using Alumina as the reference material. The test conditions were rise of 10 °C/min., Nitrogen atmosphere, temperature range for testing was room temperature to 660°C and slow cooling.

IPDT was determined from the TG values using the following method with reference to Figure 11[33].

$$IPDT = A * K * (T_f - T_i) + T_i \quad (1)$$

$$A = (S1 + S2) / (S1 + S2 + S3) \quad (2)$$

$$K = (S1 + S2) / S1 \quad (3)$$

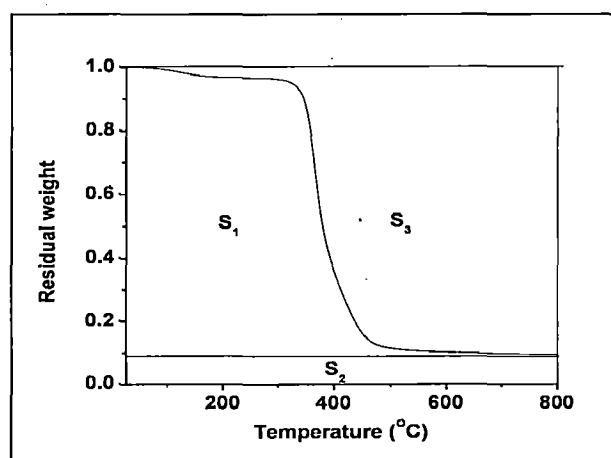


Figure 11:- Plot to determine IPDT

### 3.6 ATOMIC FORCE MICROSCOPY

AFM study was carried out for the pure epoxy, mechanical and ultrasonically mixed compositions to indirectly obtain the dispersion of nano particles in the epoxy. The instrument of AFM was NT-MDT, Ntegra operated in semi-contact (tapping) mode. The results include the Threshold grain analysis, 2D and 3D images, line analysis of the samples. The sample for AFM was also a thin piece of 5 mm x 5 mm taken from the thin film made on the petry dish. The AFM results for each composition are from at least nine samples.

### 3.7 FRACTURE SURFACE STUDY USING FE-SEM

The fractured surfaces after the tensile test was done, were carefully preserved in dessicator. Care was taken that no surface degradation occurs by any means. Small sample was cut from near the fracture surface, along the gauge length and was taken for the FE-SEM analysis. Gold particle spray was done on them to make the samples conducting. They were stick to the sample holder and a silver paint was applied along the sample. Fracture surface study is discussed in section 4.6.

### 3.8 FOURIER TRANSFORM INFRARED SPECTROSCOPY

Fourier Transform Infrared Spectroscopy (FTIR) test was carried out to study the changes in bond stretching, twisting vibrations or formation of new bond due to the presence of TiO<sub>2</sub> in the epoxy. The test was also carried out on the UV degradation tested samples to find the

presence of carbonyl group which is the cause of change in the crosslink density causing degradation of polymer. The FTIR instrument was Thermo Nicolet (Anexus). The sample for FTIR was prepared by converting the thin film of material into powder form using abrasive process.

### **3.9 ULTRAVIOLET DEGRADATION TEST**

The UV degradation test was carried out as per ASTM standard D 1435-05. This test was conducted on ultrasonically mixed composite to study the effect of UV absorption behaviour on photochemical degradation of polymers. The tensile test specimens for pure epoxy, 10, 15 and 20 wt% TiO<sub>2</sub> prepared by ultrasonic mixing were exposed to solar light for interval of 8, 16 and 24 days. After each time interval, at least three samples of each composition were tested and the percentage degradation was obtained. The test conditions for the test were UV index 7. It consists of mainly UVA and UVB radiations. The location of test was roof top of Metallurgy and Materials Engineering department Roorkee, Uttarakhand, India. The relative humidity was maximum 65% to minimum 40%. Very less amount of rainfall was there during the exposure time of 30th May 2010 to 24th June 2010.

## CHAPTER 4 RESULTS & DISCUSSION

### 4.1 Tensile Test Results for Mechanical and Ultrasonic Mixed composite

The effect of mechanical and ultrasonic mixing of TiO<sub>2</sub> nano particles in pure epoxy adhesive on the tensile strength of composite has been shown in figure 12. In case of composite prepared by mechanical mixing the addition of nano particles upto about 6 wt% lowers the

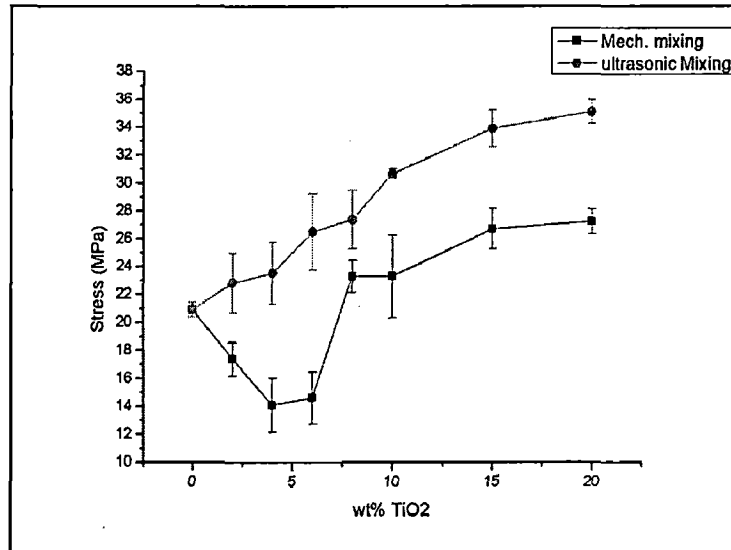


Figure 12: Variation of applied stress with wt.% TiO<sub>2</sub> addition

Strength of the composite followed by an increase in it with a further increase of the TiO<sub>2</sub> filler upto about 15 wt%. However an increase of the TiO<sub>2</sub> addition beyond this level to 20wt% shows no more significant increase in strength of the composite. The decrease in strength of the epoxy composite adhesive upto 6 wt% filler addition may have primarily attributed to formation of large agglomerates of nano particles during mechanical mixing while at higher filler content from about 8 to 20wt% possibly collide with each other and break down to smaller agglomerates upto certain extent enhancing the strength of the matrix. It is found that 6 wt% is just enough amount of filler in the epoxy which can form large agglomerates and these agglomerates are sufficiently away from each other to collide and break during mechanical mixing. This observation was supported by AFM study discussed in section 4.4. Also the large agglomerates show sign of poor bonding as per SEM study discussed in section 4.5. The ultrasonically mixed composite adhesives containing any

amount of TiO<sub>2</sub> show excellent dispersion of nano particles in the polymer matrix which may have caused increasingly higher strength exhibited by the composite with the increase in

Samples	Stress (MPa) 1 <sup>st</sup> Reading	Stress (MPa) 2nd Reading	Stress (MPa) 3rd Reading	Stress (MPa) Average
Pure Epoxy	21.47	20.52	20.68	20.89
2wt% TiO <sub>2</sub>	17.95	15.97	18.18	17.37
4wt% TiO <sub>2</sub>	16.08	14.01	12.17	14.08
6wt% TiO <sub>2</sub>	14.88	12.65	16.35	14.62
8wt% TiO <sub>2</sub>	24.33	22.05	23.47	23.28
10wt% TiO <sub>2</sub>	25.69	24.24	20	23.31
15wt% TiO <sub>2</sub>	25.84	28.36	25.88	26.69
20wt% TiO <sub>2</sub>	28.27	26.65	26.76	27.22

Table 4:- Tensile strength for Mechanically mixed composites

Samples	Stress (MPa) 1 <sup>st</sup> Reading	Stress (MPa) 2nd Reading	Stress (MPa) 3rd Reading	Stress (MPa) Average
Pure Epoxy	21.47	20.52	20.68	20.89
2wt% TiO <sub>2</sub>	25.25	21.35	21.79	22.79
4wt% TiO <sub>2</sub>	21.35	23.36	25.82	23.51
6wt% TiO <sub>2</sub>	27.47	23.25	28.70	26.47
8wt% TiO <sub>2</sub>	26.35	25.95	29.83	27.37
10wt% TiO <sub>2</sub>	30.36	30.58	31.02	30.65
15wt% TiO <sub>2</sub>	33.14	32.78	35.76	33.89
20wt% TiO <sub>2</sub>	34.14	35.35	35.77	35.08

Table 5:- Tensile strength for Ultrasonically mixed composites

filler content. The rise in strength is attributed to the resistance to crack initiation and growth in presence of the nano particles.

#### 4.2 Lap Shear Strength Results

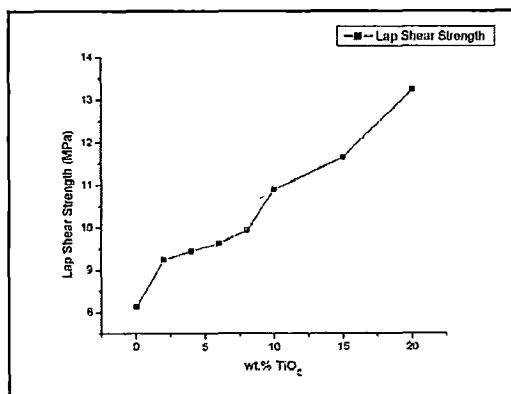


Fig. 13:- Variation of Lap Shear Strength as a function of wt.% TiO<sub>2</sub> addition for Ultrasonic Mixed samples

In view of it significantly improving the tensile strength, the lap shear strength test of the adhesive joint of aluminum was carried out only for the ultrasonically mixed composite adhesive. The variation of lap shear strength as a function of the amount of TiO<sub>2</sub> addition has been shown in Figure 13. It is found that the lap shear strength increases

With the increase in amount of filler content of the epoxy adhesive. The samples showing

Wt.% TiO <sub>2</sub>	0	2	4	6	8	10	15	20
LSS (MPa)	82.71	93.95	96.15	97.91	101.10	110.73	118.43	134.6

Table 6:- Variation of Lap Shear Strength with filler amount

Appreciable strength have been found to exhibit mixed mode of cohesive and adhesive (interface) failure. From such observations on the fracture behavior it may be assumed that till higher lap shear strength can be achieved by enhancing the adhesive strength of the interface by employing appropriate treatment to the faying surface of the substrate.

### 4.3 Glass transition and Integral Procedural Decomposition Temperatures

The Glass Transition Temperature (T<sub>g</sub>) of mechanically and ultrasonically mixed TiO<sub>2</sub> nano particle filled composites are shown in Figure 14. The figure shows that T<sub>g</sub> of composite adhesive increases with the increase in addition of TiO<sub>2</sub> nano particles by ultrasonic mixing, while in case of mechanical mixing the T<sub>g</sub> decreases with the addition of particles upto 6 wt%. The lowering of T<sub>g</sub> may have primarily attributed to the formation of large size agglomerates of nano particles which gives poor bonding with the matrix. This observation is justified quite clearly in figures 65, 66, 67 in section 4.5.

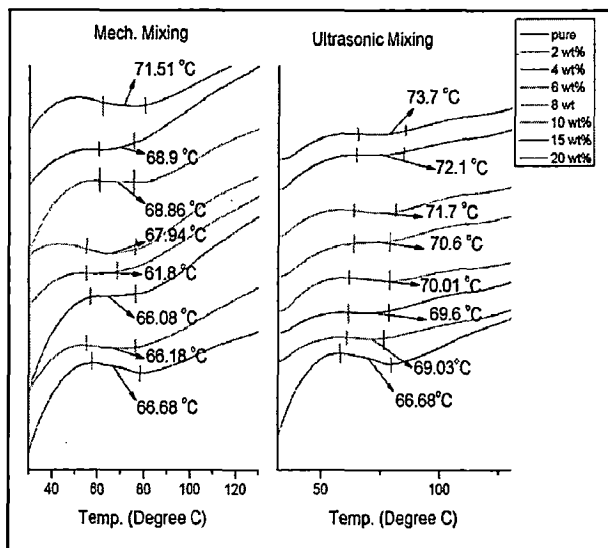


Figure 14:- T<sub>g</sub> for mechanically and Ultrasonically Prepared samples

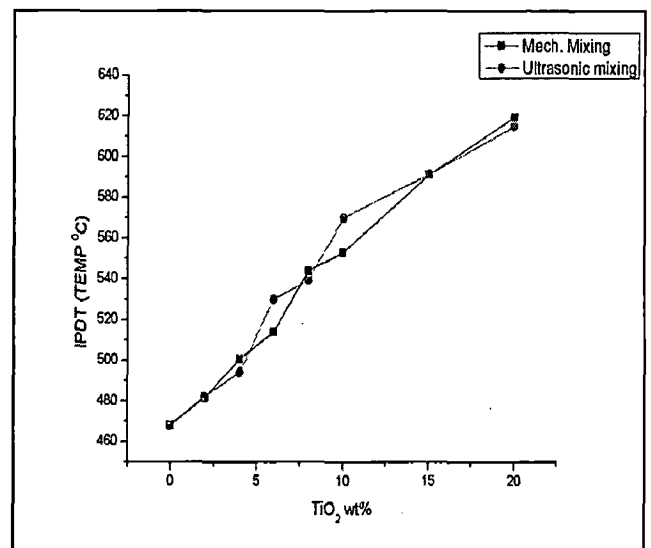


Figure 15:- IPDT variation with wt.% TiO<sub>2</sub> addition

Figure 15 shows the variation of Integral Procedural Decomposition Temperature (IPDT) with the addition of TiO<sub>2</sub> particles in case of both, mechanical and ultrasonic mixing. It is observed that the IPDT increases with the increase in amount of filler content and the rise is nearly similar for both type of mixing. The rise in IPDT shows that the thermal stability of the epoxy based composite adhesive is comparatively higher as compared to that of the pure epoxy.

Sample	S1	S2	S3	A	K	Tf	Ti	Tf-Ti	IPDT(°C)
0 Wt%	37865.43	3819.99	24315.38	0.63	1.10	660.01	29.10	630.91	467.77
2 Wt%	37647.97	4569.627	23855.13	0.64	1.12	660.73	29.01	631.72	481.64
4 Wt%	38134.47	5236.627	22640.02	0.66	1.14	660.11	29.05	631.06	500.61
6 Wt%	38292.89	5768.839	21951.12	0.67	1.15	660.13	29.11	631.02	513.75
8 Wt%	38930.3	6853.763	20235.96	0.69	1.18	660.20	29.18	631.02	543.83
10 Wt%	39160.95	7158.758	19707.88	0.70	1.18	660.28	29.11	631.16	552.83
15 Wt%	39680.57	8613.967	17729.14	0.73	1.22	660.24	29.18	631.06	590.99
20 Wt%	39944.52	9709.843	16377.77	0.75	1.24	660.32	29.13	631.19	619.15

Table 7:- IPDT results for Mechanically mixed composites

Sampl e	S1	S2	S3	A	K	Tf	Ti	Tf-Ti	IPDT(°C)
0 Wt%	37865.4	3819.99	24315.3	0.63	1.10	660.0	29.10	630.91	467.77
2 Wt%	39169.4	3854.83	23373.2	0.65	1.10	663.9	33.18	630.79	482.15
4 Wt%	39674.7	4612.47	23371.5	0.65	1.12	663.9	33.03	630.92	494.03
6 Wt%	40263.0	5621.97	20511	0.69	1.14	663.9	33.11	630.85	529.95
8 Wt%	40349.4	6002.02	20040.3	0.70	1.15	663.9	33.01	630.90	539.00
10 Wt%	41226.3	7034.59	18132.2	0.73	1.17	663.9	33.00	630.93	569.88
15 Wt%	41168.7	7202.46	15860.4	0.75	1.17	663.9	33.03	630.95	591.31
20 Wt%	41712.2	8821.27	15862.3	0.76	1.21	663.9	33.05	630.91	614.78

Table 8:- IPDT results for Ultrasonically mixed composites

The thermal stability was also characterized as the temperature measurement as a function of residual weight, amount of filler addition and the method of mixing as shown in figure 16, at a given heating rate of 10 °C/min. In case of ultrasonic mixing the loss of mass of composite

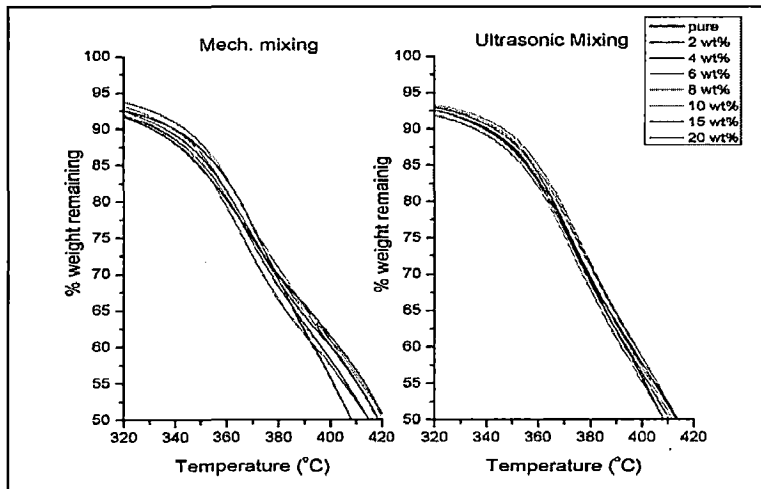


Figure 16:- Percentage residual weight as a function of filler amount, method of mixing and temperature

Has insignificant influence of the amount of TiO<sub>2</sub> addition (upto 20 wt%), till the temperature of the order of 375 ± 1 °C, and 391 ± 1 °C in mechanical mixing. However at higher temperature range upto 563 °C and upto 461 °C in mechanical mixing, the stability of composite has been found to improve with the increase in TiO<sub>2</sub> addition to it as shown in table 9 and 10.

Residual wt. (%)	Amount of TiO <sub>2</sub> addition (wt%)							
	0	2	4	6	8	10	15	20
	Exposure Temperature (Degree C)							
90	333.93	328.6	333.52	334.44	339.4	341.52	337.75	334.55
80	363.49	361.78	362.72	364.34	365.86	367.01	364.42	363.58
70	377.66	375.8	376.98	378.17	380.11	380.8	378	378
60	391.8	390.36	392.32	393.53	395.67	396.19	394.39	393.69
50	406.9	406.98	408.95	410.32	412.08	412.26	411.66	412.08
40	420.39	422.34	423.53	425.2	426.41	427	427	427.59
30	432.46	435.65	436.49	438.33	439.33	440.16	441.25	442.35
20	444.76	449.03	450.13	452.32	453.93	455.27	458.56	461.95

Table 9:- Percentage residual weight related to filler amount and temperature for mechanical mixing

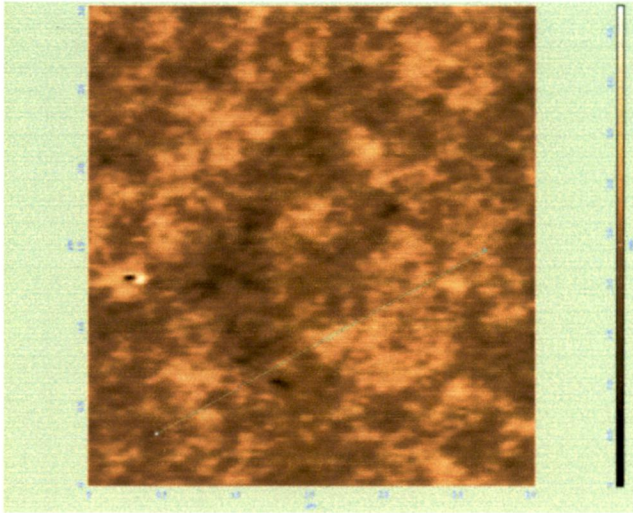
Residual wt. (%)	Amount of TiO <sub>2</sub> addition (wt%)							
	0	2	4	6	8	10	15	20
	Exposure Temperature (Degree C)							
70	377.66	372.27	375.3	376.64	377.24	379.61	377.4	377.58
60	391.8	391.8	394.48	397.88	398.39	399.76	401.13	400.18
50	406.9	413.2	413.2	417.09	417.18	418.96	419.8	419.89
40	420.39	429.19	428.94	431.54	431.7	433.64	434.56	435.9
30	432.46	443.83	443.09	444.77	446.19	447.11	451.15	455.02
20	444.76	460.17	461.01	465.13	468.21	487.56	549.84	563.52

Table 10:- Percentage residual weight related to filler amount and temperature for ultrasonic mixing

#### 4.4 ATOMIC FORCE MICROSCOPY (AFM) RESULTS

AFM was carried out for the mechanically mixed samples to find out the surface topography, particle distribution and to find agglomerate formation and its size. AFM results also support the decrease in tensile strength for 2, 4 and 6 wt% TiO<sub>2</sub> addition in epoxy adhesive by showing the presence of agglomerates of larger size in these composite adhesives. For each sample there are 3 sub-samples and from each sub-sample there are 3 more AFM samples. Thus total 9 samples are there for each wt% addition. The results are the average of 9 samples per each wt% addition and the best image is shown below for each wt% addition sample.





**Fig 17. 2D AFM image of pure epoxy**

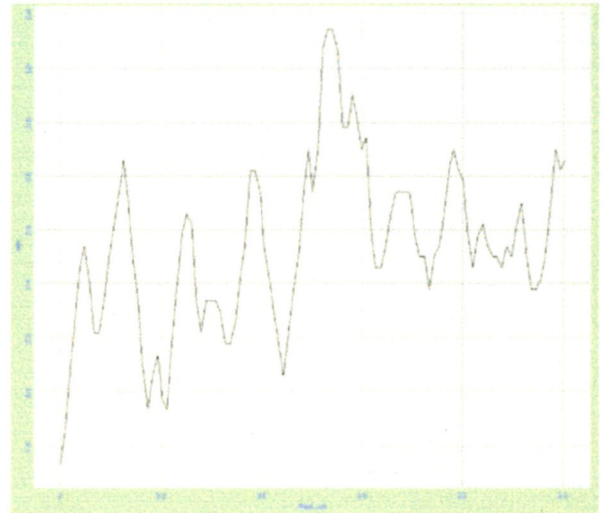


**Fig 18. Line analysis of pure epoxy**



**Fig 19. 3D image of pure epoxy**

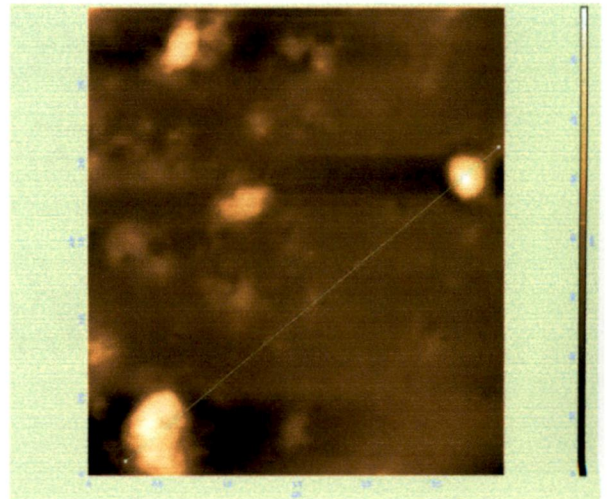


**Fig 20. 2D AFM image of 2 wt% mech. mixed TiO<sub>2</sub> added composite**

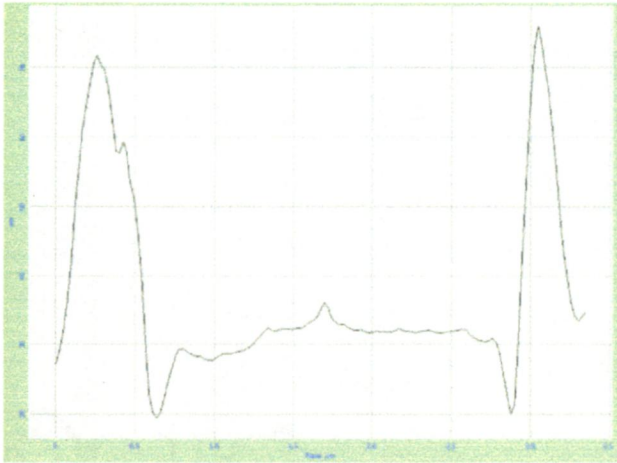


**Fig 21. Line Analysis of 2 wt.% mech. Mixed TiO<sub>2</sub> composite**

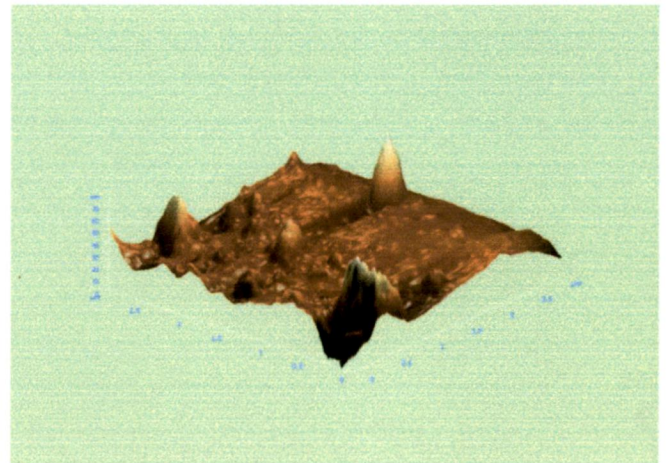


**Fig 22. 3D AFM image of 2 wt.% mech. Mixed TiO<sub>2</sub> composite**

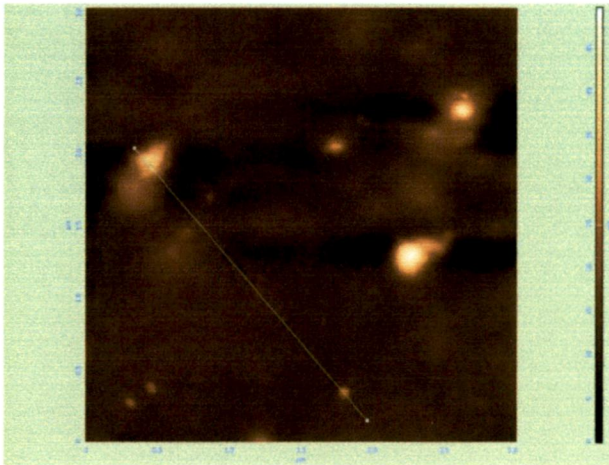


**Fig 23. 2D AFM image of 4 wt.% mech. Mixed composite**

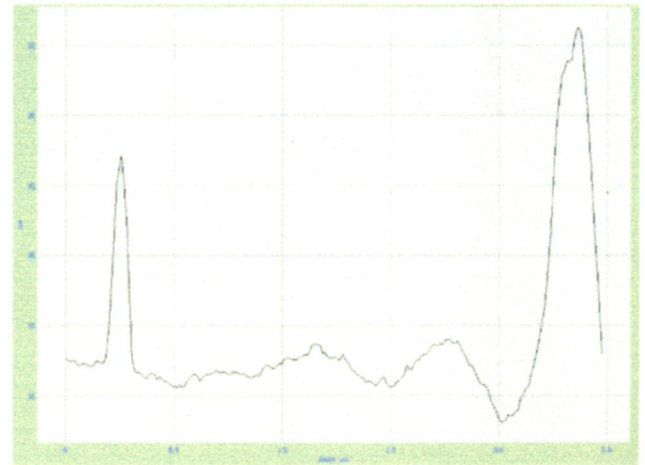


**Fig 24. Line analysis of 4 wt.% mech. mixed composite**



**Fig 25. 3D AFM image of 4 wt.% Mech. Mixed composite**

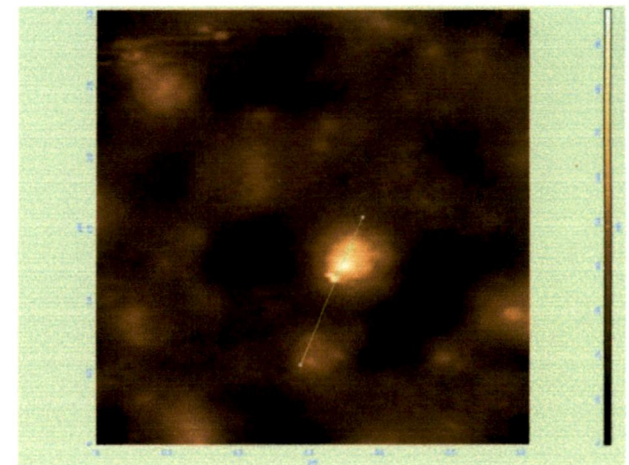


**Fig 26. 2D AFM image of 6 wt.% mech. Mixed composite**

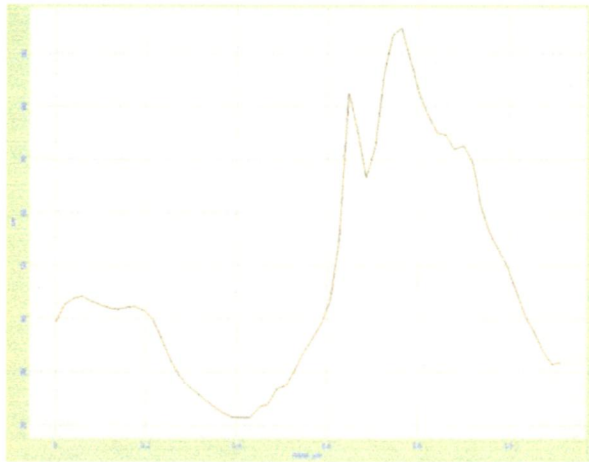


**Fig 27. Line analysis of 6 wt.% mech. Mixed composite**

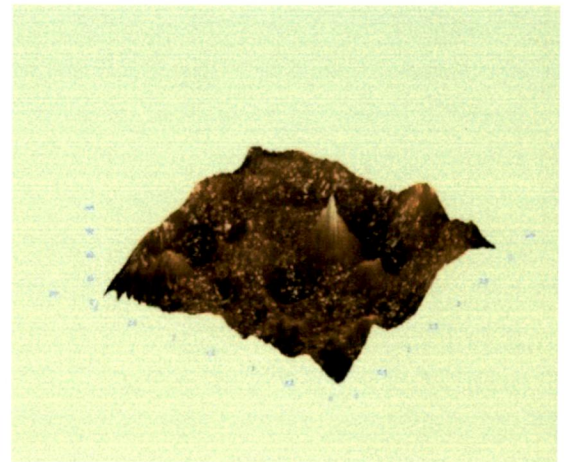


**Fig 28. 3D AFM image of 6 wt.% mech. Mixed composite**

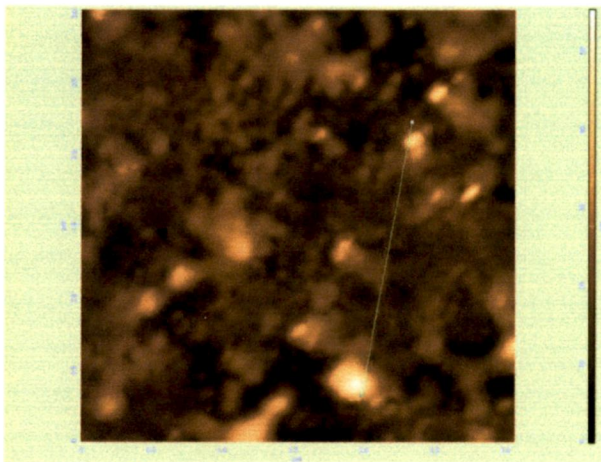


**Fig 29. 2D AFM image of 8 wt.% mech. Mixed composite**

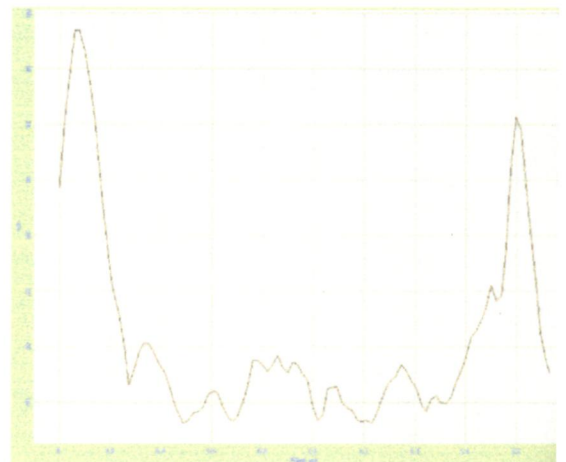


**Fig 30. Line analysis of 8 wt.% mech. mixed composite**

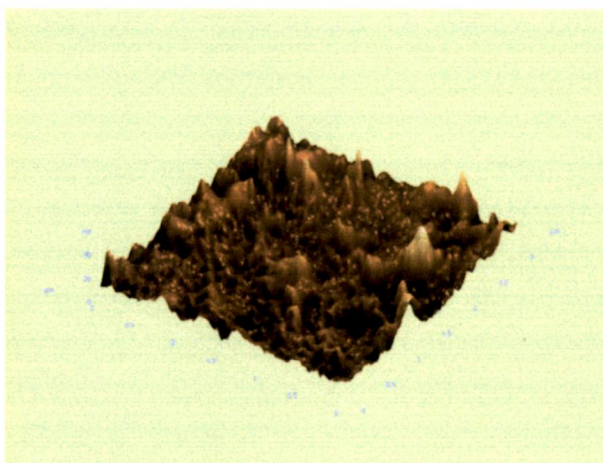


**Fig 31. 3D AFM image of 8 wt.% Mech. Mixed composite**

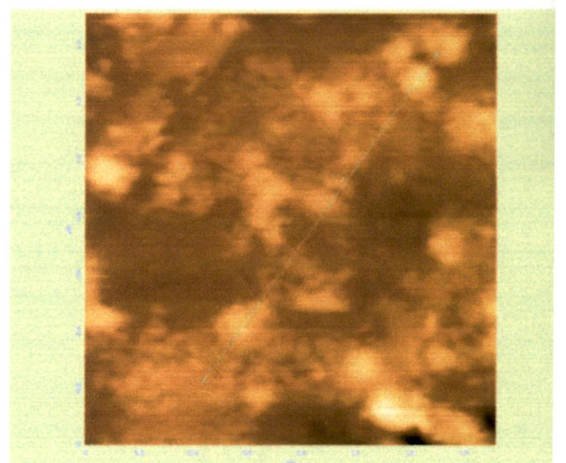


**Fig 32. 2D AFM image of 10 wt.% mech. Mixed composite**

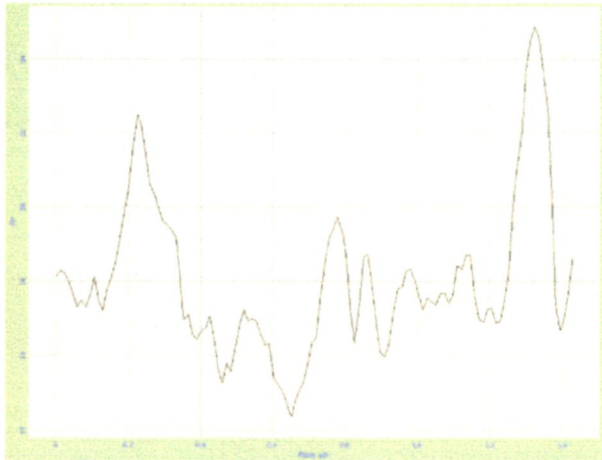


**Fig 33. Line analysis of 10 wt.% TiO<sub>2</sub> mech. Mixed composite**

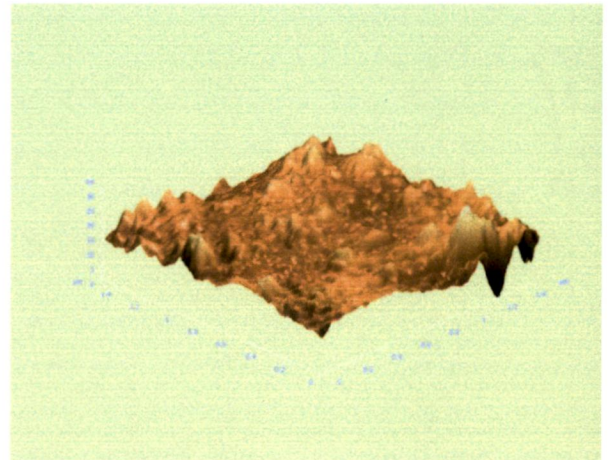


**Fig 34. 3D AFM image of 10 wt.% TiO<sub>2</sub> mech. Mixed composite**

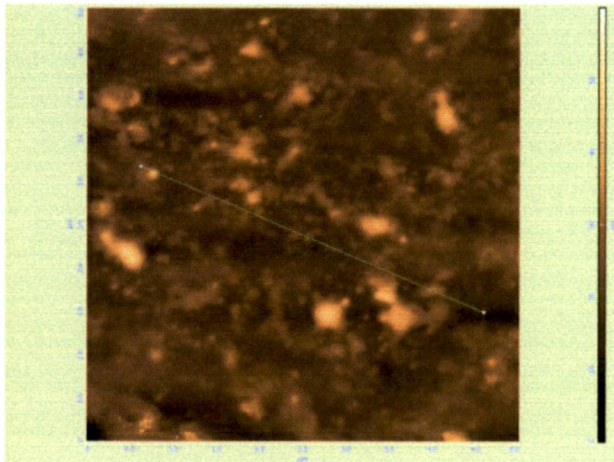


**Fig 35. 2D AFM image of 15 wt.% Mech. Mixed composite**

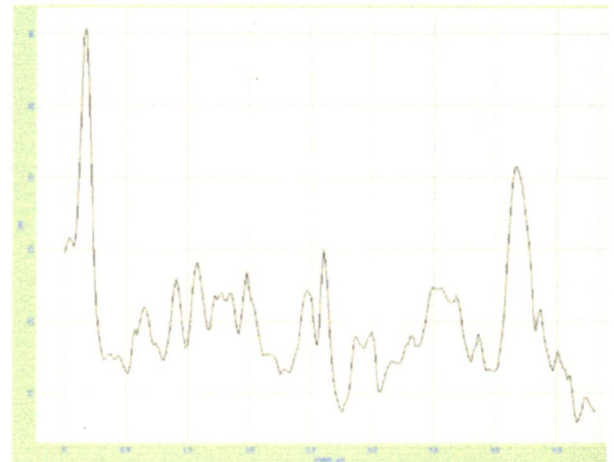


**Fig 36. Line analysis of 15 wt.% mech. Mixed composite**

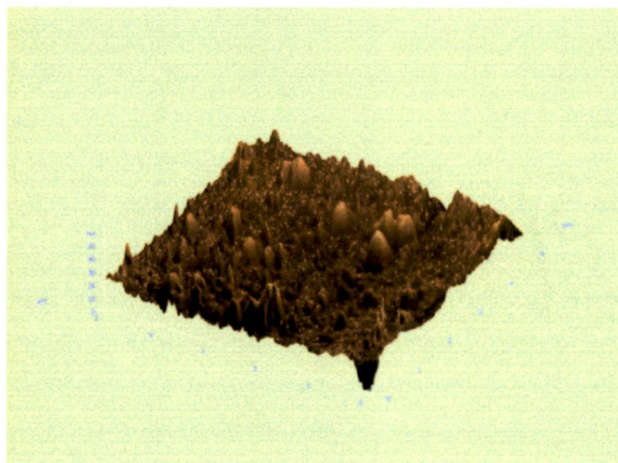


**Fig 37. 3D AFM image of 15 wt.% Mech. Mixed composite**

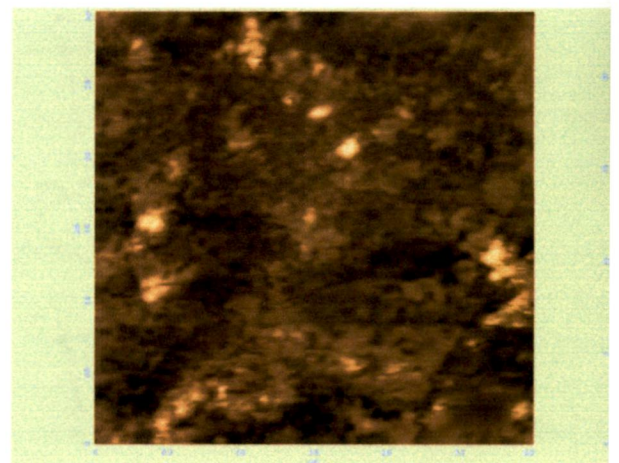


**Fig 38. 2D AFM image of 20 wt.% mech. Mixed composite**

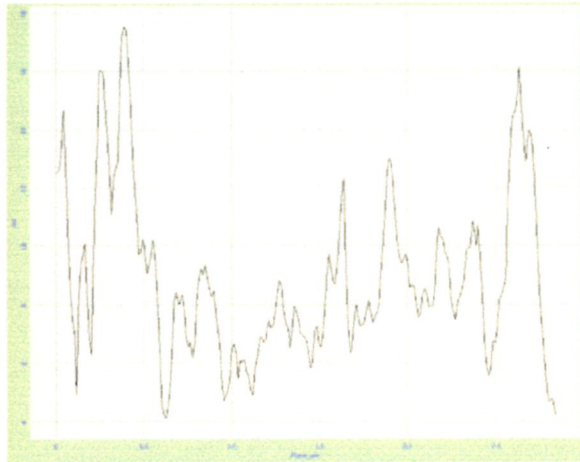


**Fig 39. Line analysis of 20 wt.% mech. Mixed composite**

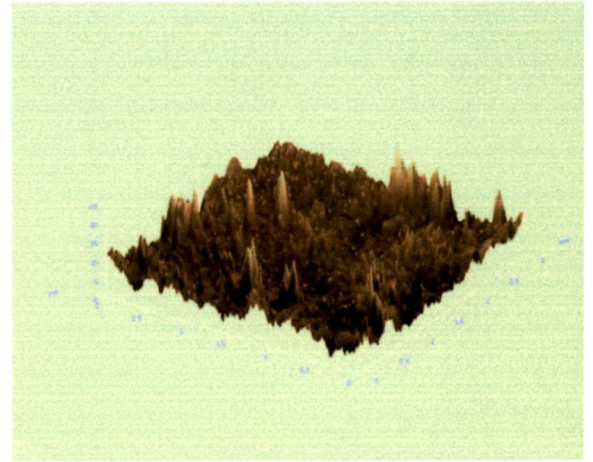


**Fig 40. 3D AFM image of 20 wt.% mech. Mixed composite**

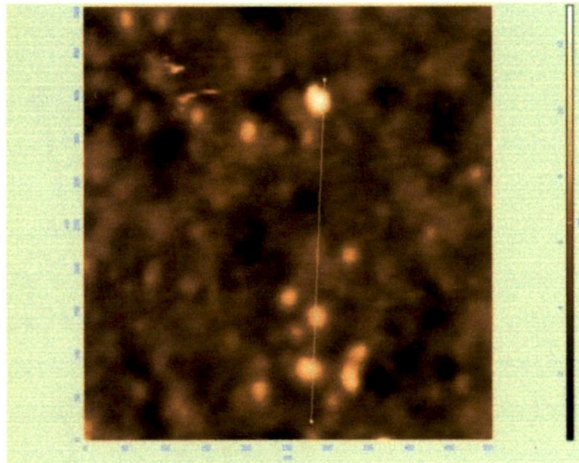


**Fig 41. 2D AFM image of 2 wt.% ultrasonically mixed composite**

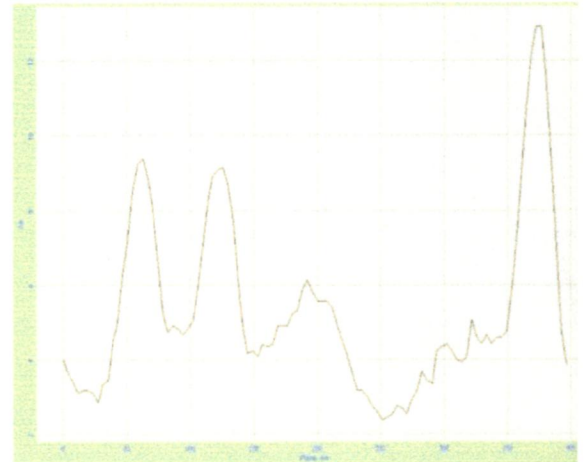


**Fig 42. Line analysis of 2 wt.% ultrasonically Mixed composite**

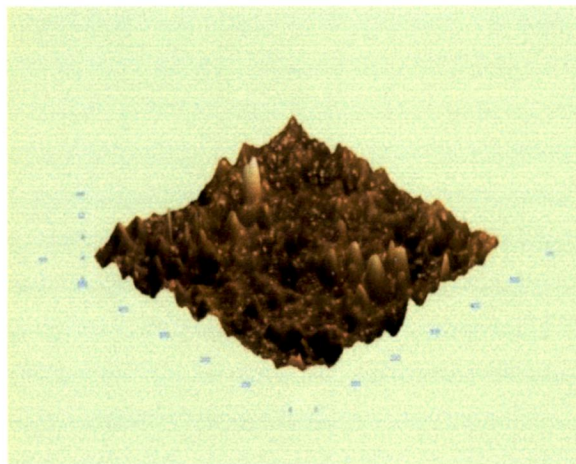


**Fig 43. 3D AFM image of 2 wt.% ultrasonically mixed composite**

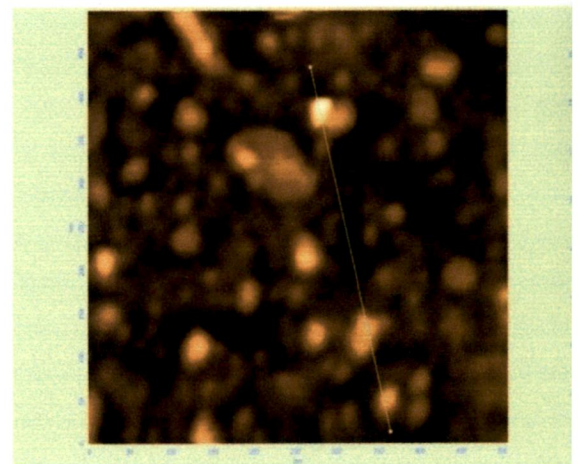


**Fig 44. 2D AFM image of 4 wt.% ultrasonically Mixed composite**

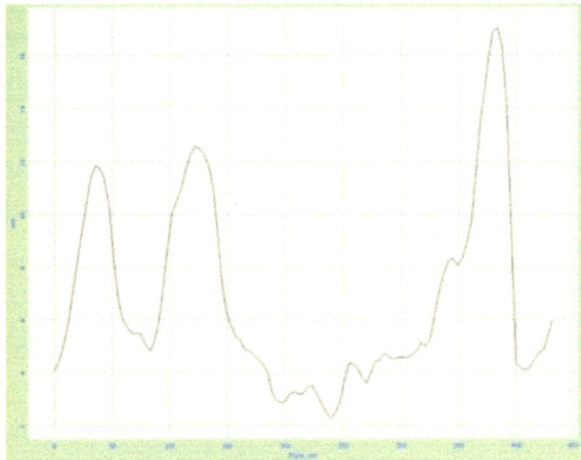


**Fig 45. Line analysis of 4 wt.% ultrasonically mixed composite**

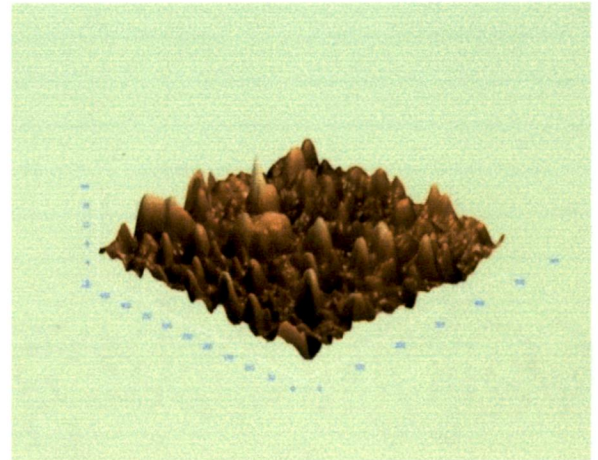


**Fig 46. 3D AFM image of 4 wt.% ultrasonically Mixed composite**

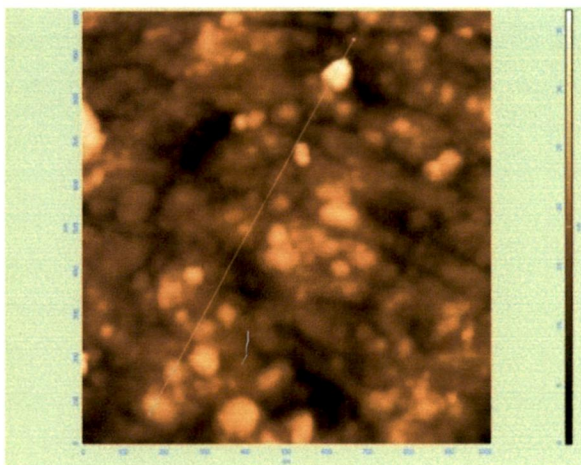


**Fig 47. 2D AFM image of 6 wt.% ultrasonically mixed composite**

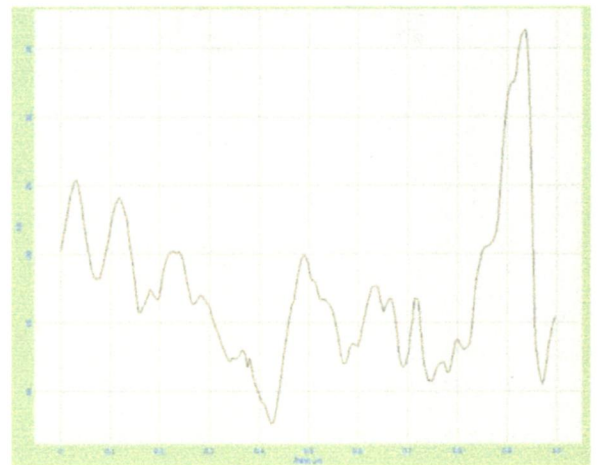


**Fig 48. Line analysis of 6 wt.% ultrasonically Mixed composite**

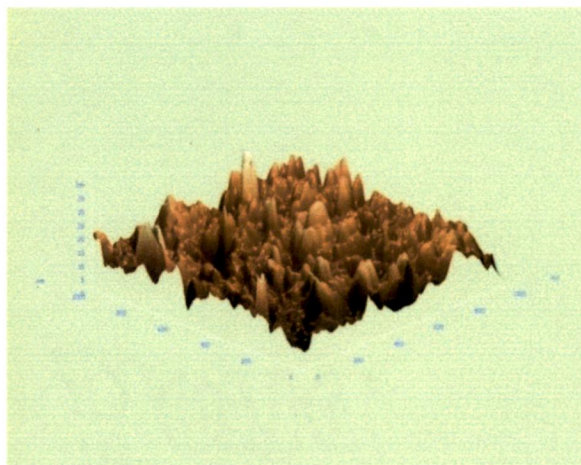


**Fig 49. 3D AFM image of 6 wt.% ultrasonically mixed composite**

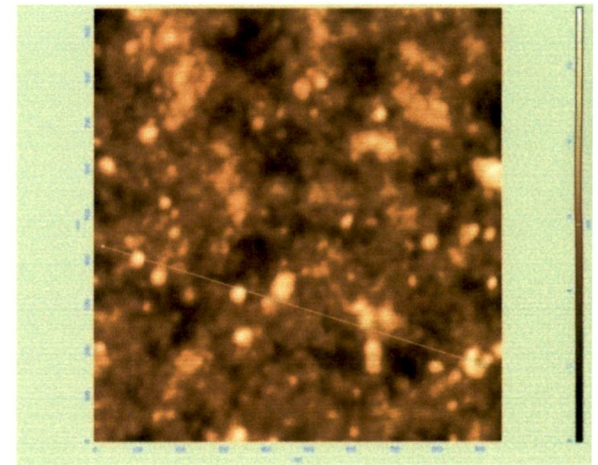


**Fig 50. 2D AFM image of 8 wt.% ultrasonically Mixed composite**

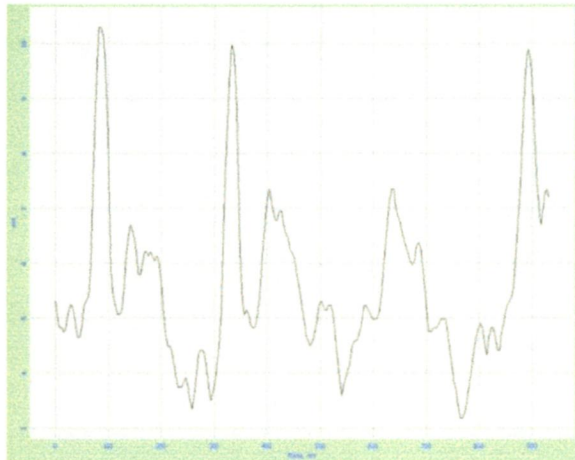


**Fig 51. Line analysis of 8 wt.% ultrasonically mixed composite**

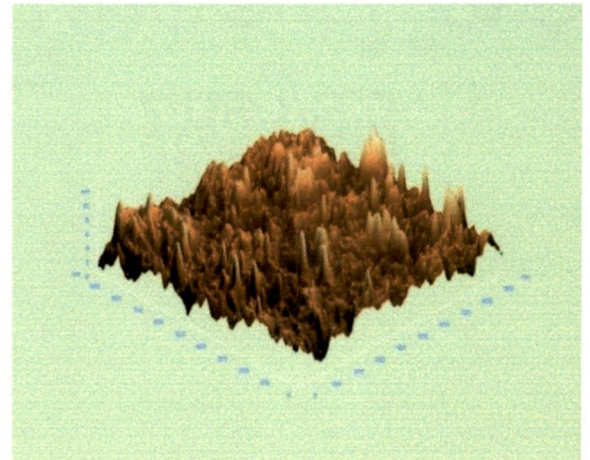


**Fig 52. 3D AFM image of 8 wt.% ultrasonically Mixed composite**

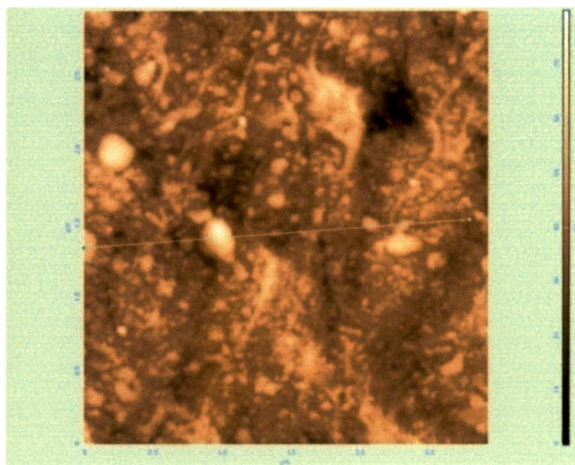


**Fig 53. 2D AFM image of 10 wt.% ultrasonically mixed composite**

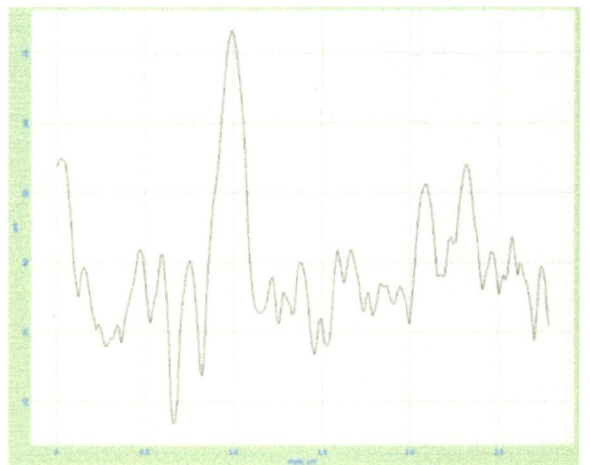


**Fig 54. Line analysis of 10 wt.% ultrasonically Mixed composite**

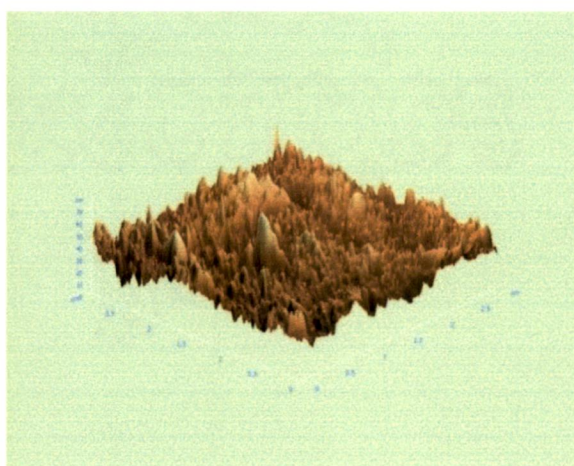


**Fig 55. 3D AFM image of 10 wt.% ultrasonically mixed composite**

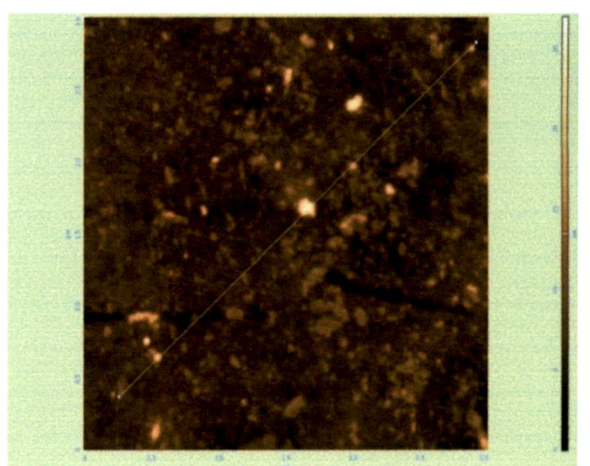


**Fig 56. 2D AFM image of 15 wt.% ultrasonically Mixed composite**

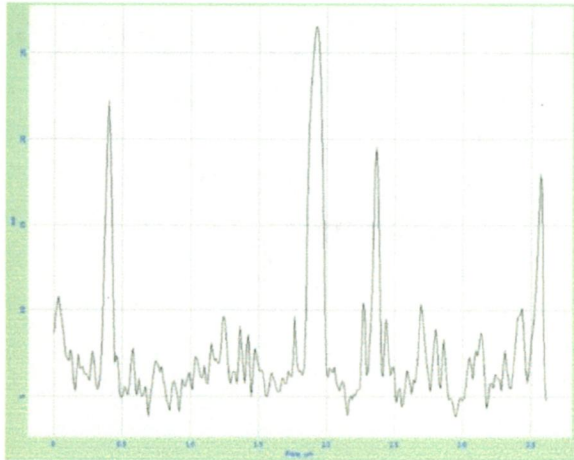


**Fig 57. Line analysis of 15 wt.% ultrasonically mixed composite**

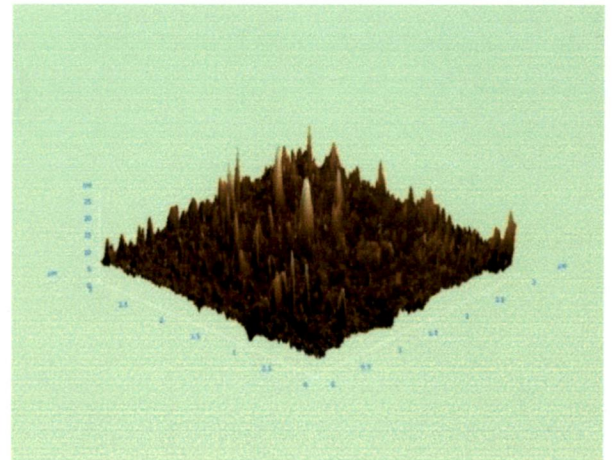


**Fig 58. 3D AFM image of 15 wt.% ultrasonically Mixed composite**

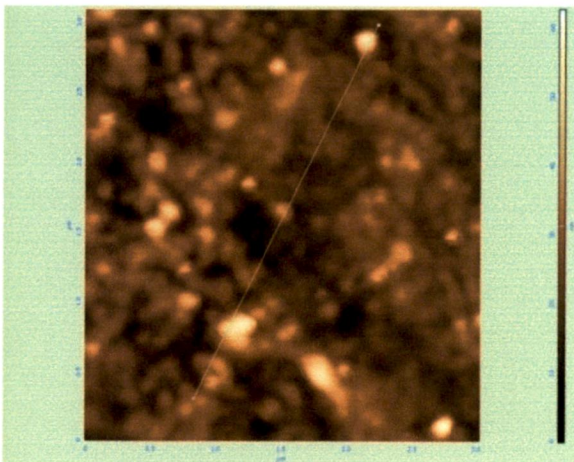


**Fig 59. 2D AFM image of 20 wt.% ultrasonically mixed composite**

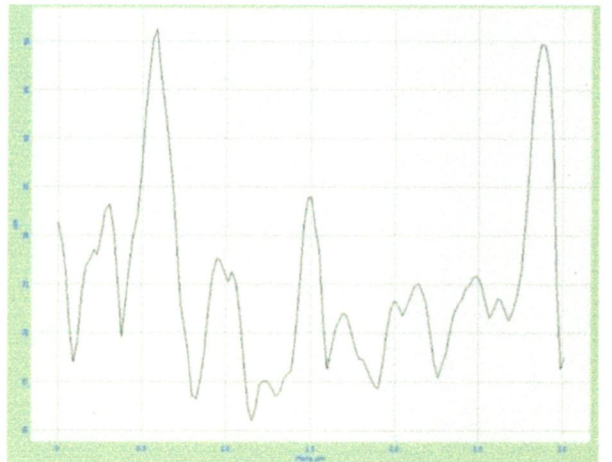


**Fig 60. Line analysis of 20 wt.% ultrasonically Mixed composite**

The analysis of AFM images gives a crude idea about the distribution of nano particles in the composite adhesive near the surface. The analysis of mechanically mixed composite show

that as we go from pure epoxy towards 20wt% addition composite, agglomerates of bigger size reduces and smaller size agglomerate increases. Figure 17, 18, 19 show that the plain epoxy surface is surface roughness of approximately 30 nm. Figure 20, 21, 22 show large agglomerates formation with high surface roughness and the

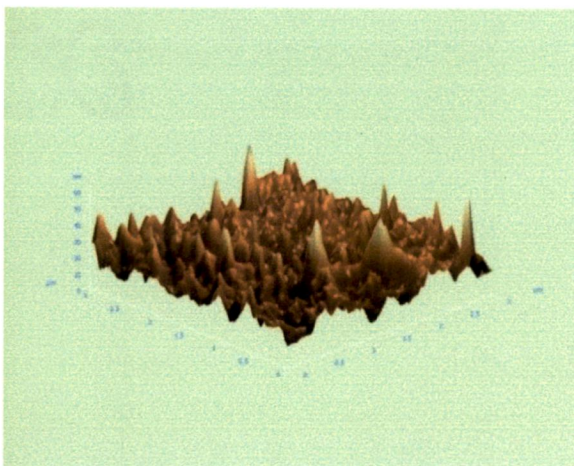


**Figure 61:- 3D AFM image of 20 wt% ultrasonically mixed composite**



distance and size of agglomerates increases as we go for 4 and 6 wt% filler addition which is shown subsequently in Figures 23, 24, 25, 26, 27 and 28. Figure 29, 30 and 31 show that amount of smaller agglomerates increase in number for a given area of composite with reduced surface roughness. As we study the AFM images for 10, 15 and 20 wt% it becomes apparently clear that the large agglomerates are decreasing in number and smaller are increasing with lesser surface roughness which is shown in figures 32 to 40. The same has been confirmed by the following analysis. Nine samples of each wt% addition are studied for the approx. agglomerate size by taking the area from the image covered by the particles. We divide the area of agglomerate by area of single nano-particle (found by considering the nano-particles spherical in nature and of diameter 25 nm). The area of one particle comes to 490.625 nm<sup>2</sup>. In this way a whole frequency distribution table is prepared for each wt% addition sample and a trend was obtained about the size of agglomerates found in the samples. For e.g. one figure is explained below.

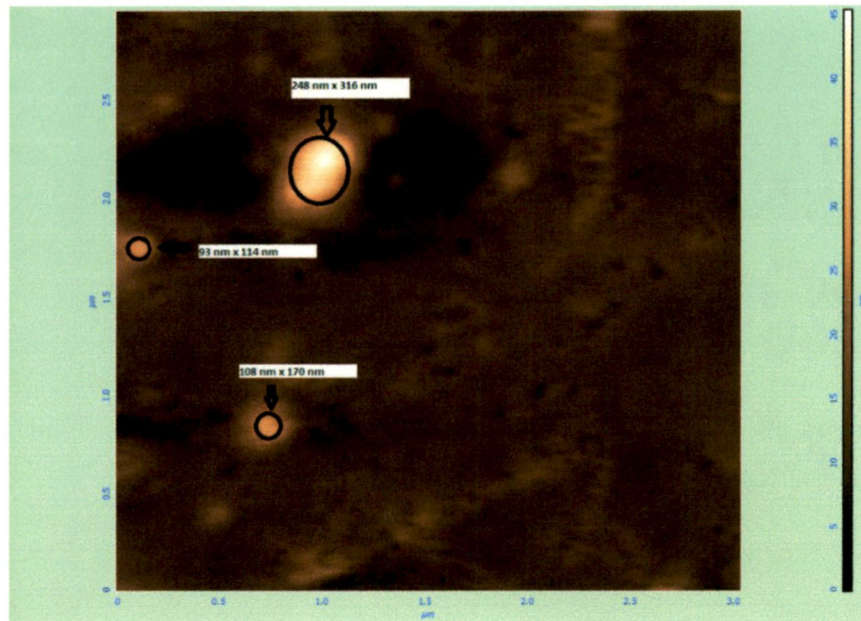


**Figure 62:- AFM image of 4 wt% showing the analysis of particle agglomerate size**

- ✓ In above figure we can see that there are 3 agglomerates of particles with size
- ✓ a)  $108 \times 170 = 18360 \text{ nm}^2$
- ✓ Area of one nano particle is  $490.625 \text{ nm}^2$
- ✓ So the size of agglomerate is  $\{18360 / 490.625\} = 37.42$  particles in the agglomerate.
- ✓ In similar manner other agglomerate particle size are determined and following results are obtained.

PARTICLE AGGLOMERATE SIZE	2 WT%	4 WT%	6 WT%	8 WT%	10 WT%	15 WT%	20 WT%
1 to 20	0	1	0	6	6	11	14
20 to 40	0	0	1	7	7	10	8
41 to 70	5	3	4	6	6	8	6
70 to 100	0	8	3	2	2	2	1
101 to 300	4	9	11	0	0	0	0
301 to 600	1	0	4	0	0	0	0

Table 11:- Details of Particle agglomerate size in 9 samples per wt% addition as per AFM analysis

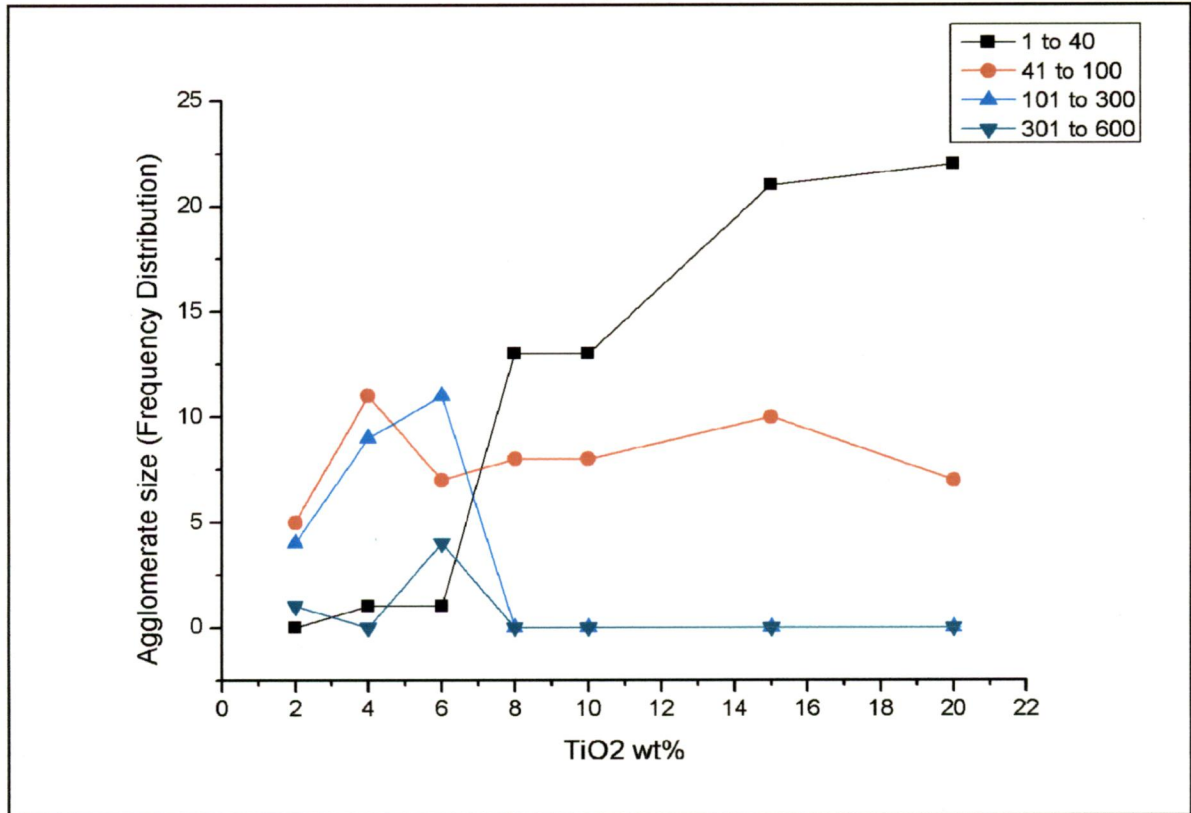


Figure 63:- Agglomerate Size (Frequency Distribution) as function of filler addition

### INFERENCES FROM ABOVE FIGURE

As we can see from the above figure that from lower wt% to higher wt% addition samples, the Frequency Distribution of agglomerate size increases for small size agglomerates (1 to 40) of particles. For (40 to 100) agglomerate size, the frequency distribution remains about 5 to 10 on an average, for the entire range of filler addition. As we go towards higher agglomerate size of particles (100 to 300) and (300 to 600) we find that they are present only

in 2, 4 and 6 wt% and absent for higher filler additions. The reason being, on mechanically mixing the nano-particles in the epoxy, the number of particles is higher in 8, 10, 15 and 20 wt% addition, hence even if the agglomerates of large size form, they collide with each other and break into small agglomerates, but in 6 wt% addition the particles are just enough to form large size agglomerates and still sufficiently away not to collide with each other and break into smaller agglomerates. In 2 and 4 wt% addition composite the nano-particles are not enough to form extremely large size agglomerate of particles (300 to 600) so they do not show the presence of such large particles. Also the agglomerates of (1 to 40) size are not much found in these samples as the agglomerates formed are sufficiently away from each other in the epoxy to collide and break. If at all they collide, then they do not have enough energy to break due to the high viscosity of epoxy. Thus in 2 and 4 wt% samples we find maximum agglomerate size particles present in the range of (40 to 100) and (100 to 300). This analysis supports the Tensile Strength data shown in section 4.1. The study of AFM images of ultrasonically mixed composites from 2 to 20 wt% filler addition show excellent dispersion of nano particles in the matrix, which is clearly apparent from the figures 41 to 61 which are 2D, line analysis and 3D images for 2,4,6,8,10,15 and 20 wt% filler addition respectively. All images clearly show impact of ultrasonic cavitation phenomena on effectively breaking the agglomerates.

#### 4.5 FRACTURE SURFACE STUDY

The fracture surface of tensile test specimens of mechanically and ultrasonically mixed composites were studied using FE-SEM to understand the effect of addition of filler on the fracture behavior of polymer. Also the fracture surfaces of lap shear specimens for ultrasonically mixed composites were also studied. **Figure 64** below shows the multiple point fracture pattern of pure polymer. Also for 2, 4 and 6 wt% filler addition by mechanical mixing shows the formation of large agglomerates of particles at distant locations in the matrix as shown in fig. 65, 66, 67. These agglomerates exhibit very poor bonding with the matrix and as a result the mechanical and thermal properties have degraded to a large extent.



Figure 64:- Fracture surface image of pure epoxy

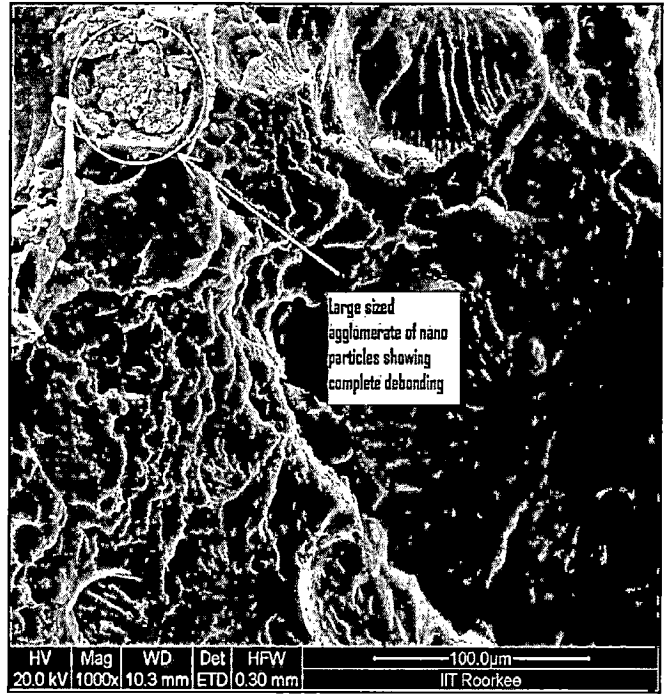


Fig. 65:- Fracture surface image of 2 wt.% mech. Mixed composite

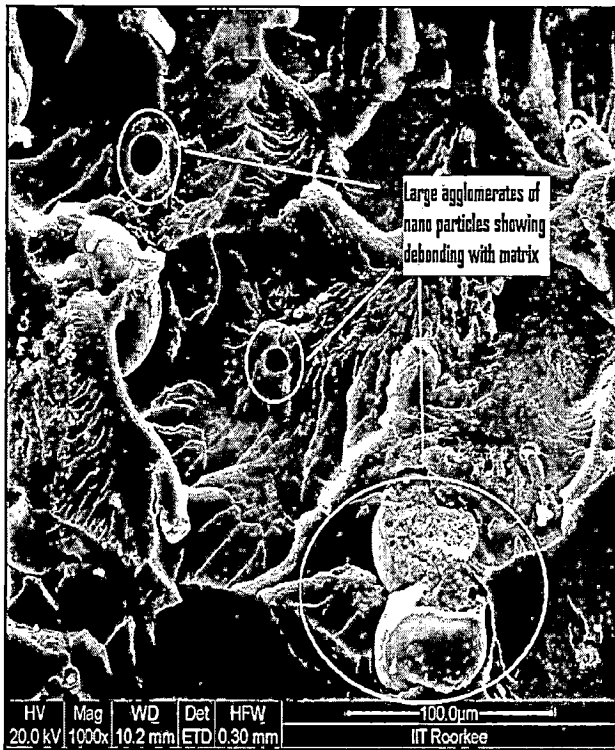


Fig. 66:- Fracture surface image of 4 wt.% Mech. mixed composite



Fig. 67:- Fracture surface image of 6 wt.% mech. mixed composite

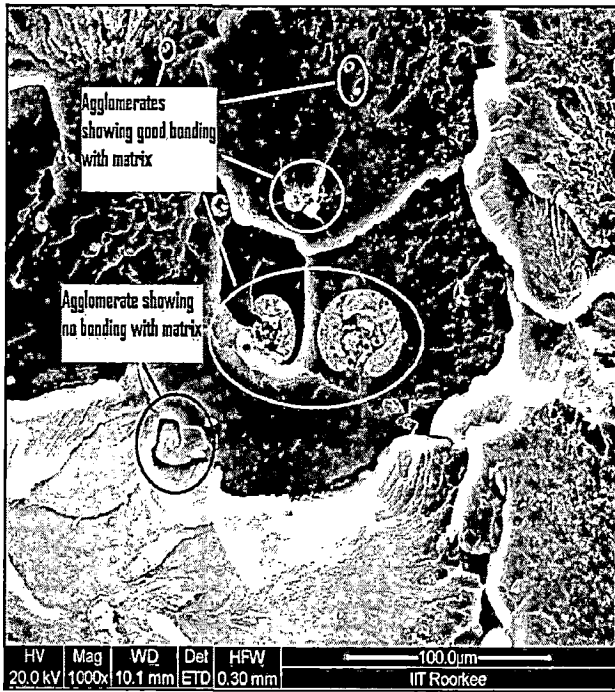


Figure 68:- Fracture surface image of 8 wt.% mech. Mixed composite



Figure 69:- Fracture surface image of 10 wt.% mech. Mixed composite

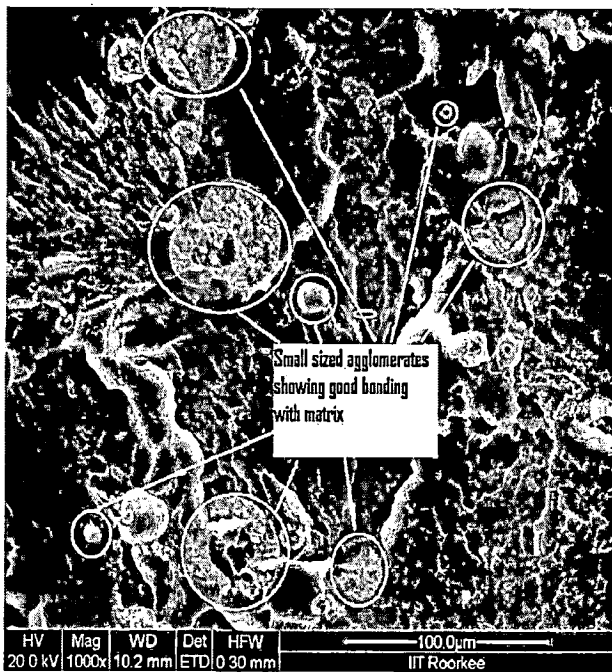


Figure 70:- Fracture surface image of 15 wt.% mech. Mixed composite

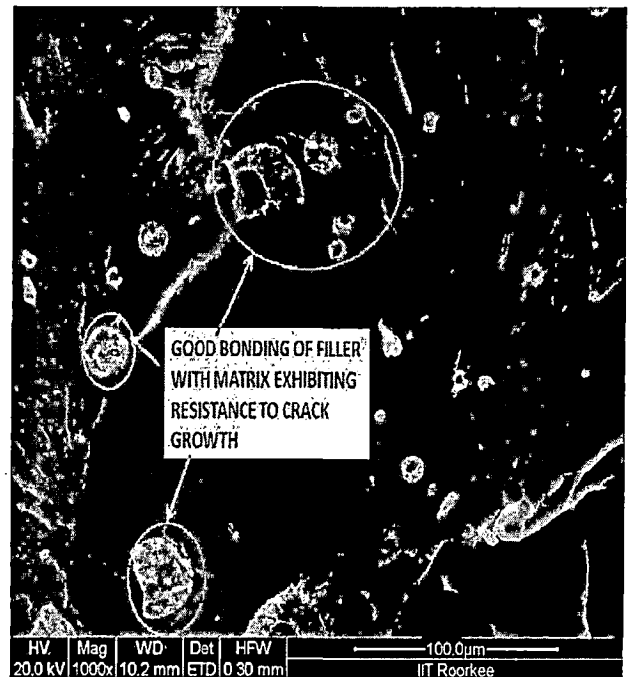


Figure 71:- Fracture surface image of 20 wt.% mech. Mixed composite

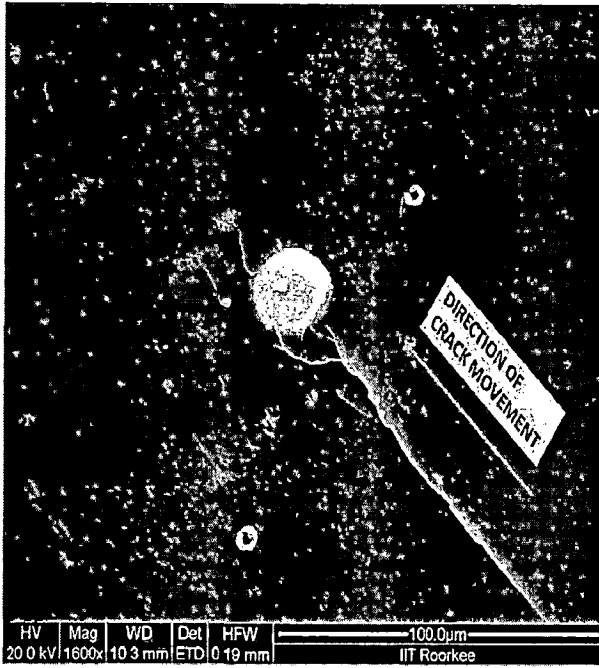


Figure 72:- Fracture image of 15 wt.% mech. Mixed composite at higher magnification



Figure 73:- Fracture image of 20 wt.% mech. Mixed composite at higher magnification



Figure 74:- Fracture surface image of 2 wt.% ultrasonically mixed composite

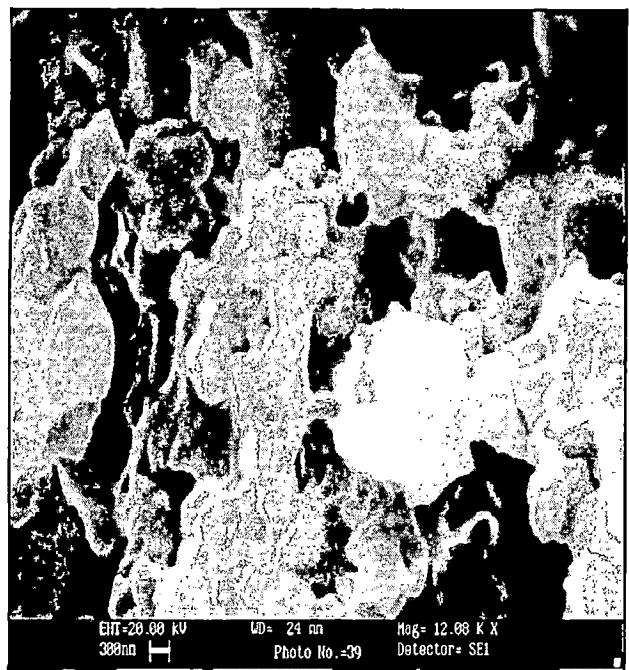


Figure 75:- Fracture surface image of 4 wt.% ultrasonically mixed composite

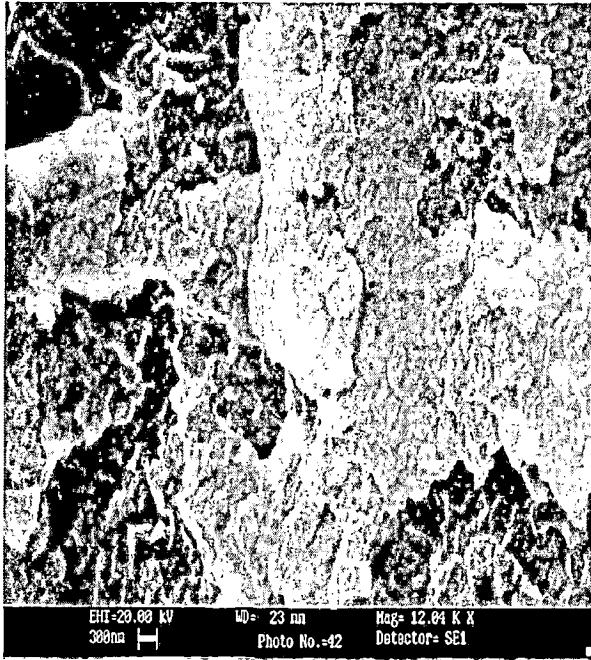


Fig. 76:- Fracture surface image of 6 wt.% ultrasonically mixed composite

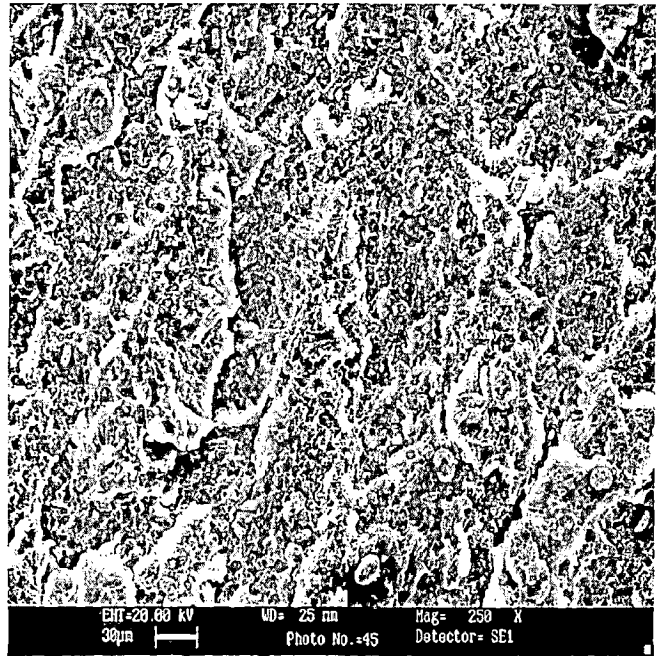


Fig. 77:- Fracture surface image of 8 wt.% ultrasonically mixed composite



Fig. 78:- Fracture surface image of 8 wt.% ultrasonically mixed composite at higher magnification

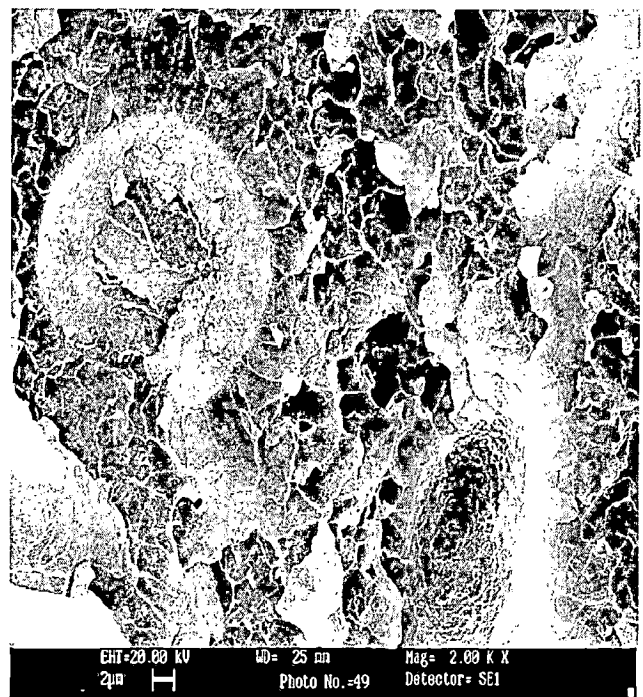


Fig. 79:- Fracture surface image of 10 wt.% ultrasonically mixed composite



Fig. 80:- Fracture surface image of 10 wt.% ultrasonically mixed composite at higher magnification

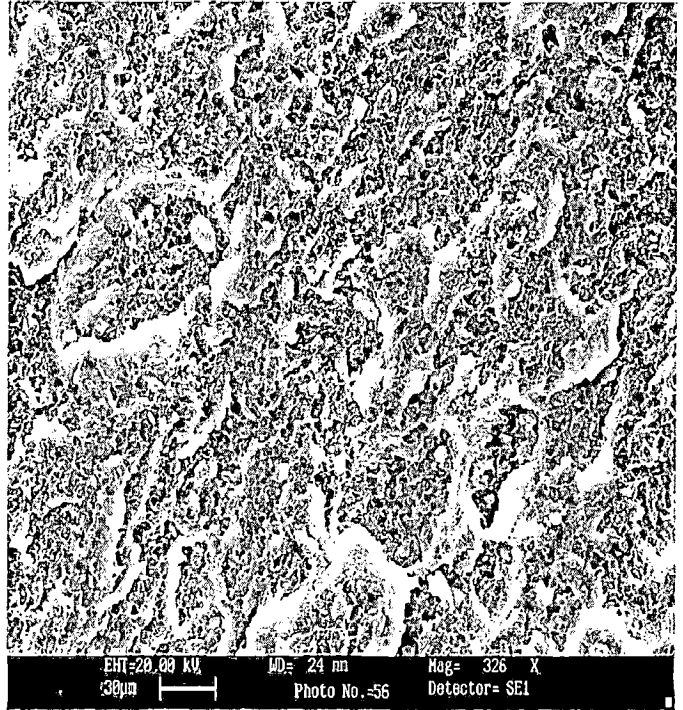


Fig. 81:- Fracture surface image of 15 wt.% ultrasonically mixed composite



Fig. 82:- Fracture surface image of 15 wt.% ultrasonically mixed composite at higher magnification

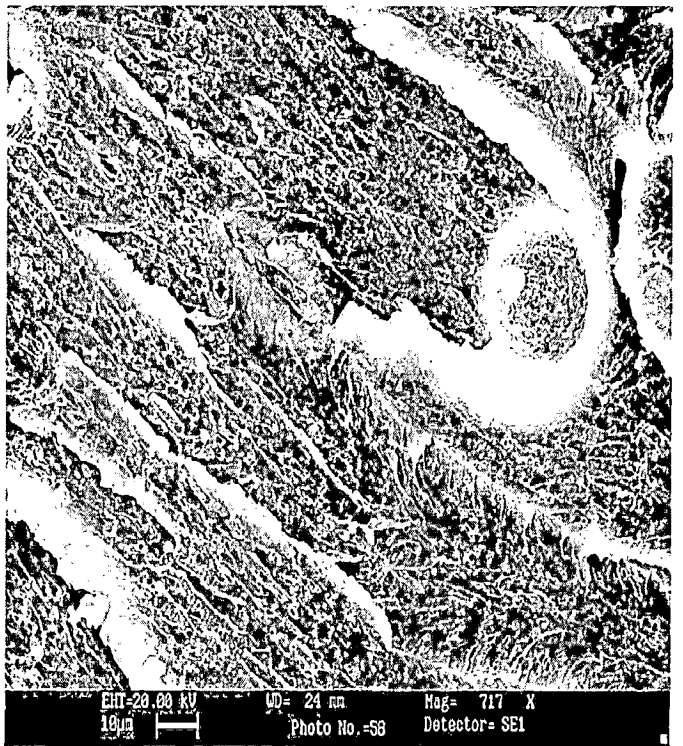


Fig. 83:- Fracture surface image of 20 wt.% ultrasonically mixed composite





Fig. 84:- Fracture surface image of 20 wt.% ultrasonically mixed composite at higher magnification

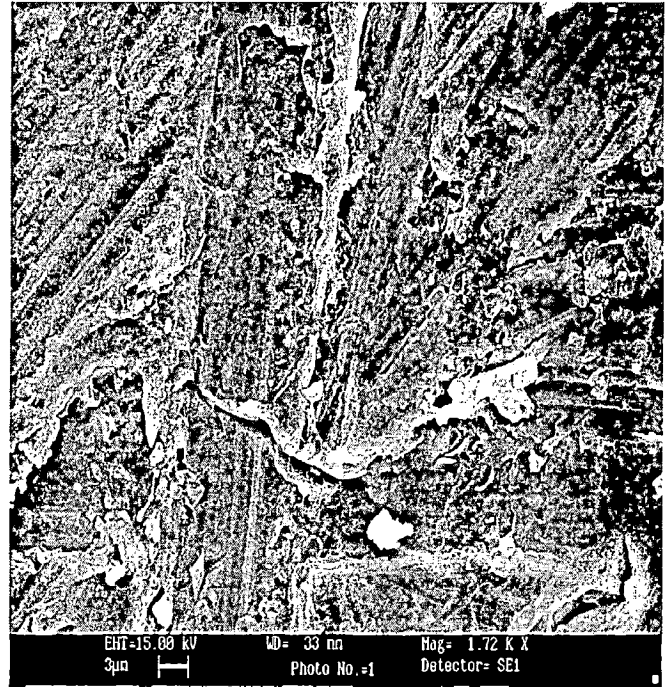


Fig. 85:- Fracture image of pure epoxy (Lap Shear specimen)



Fig. 86:- Fracture image of 2 wt.% ultrasonically mixed composite (Lap Shear Specimen)

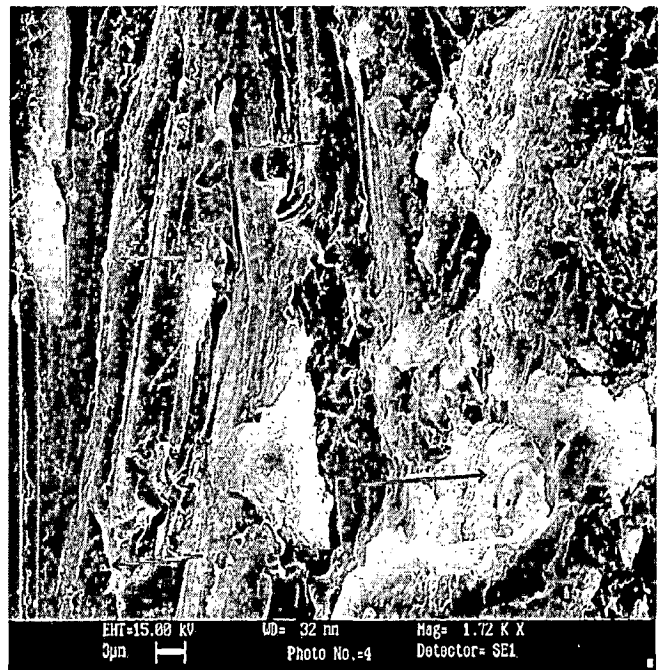


Fig. 87:- Fracture image of 4 wt% ultrasonically mixed composite (Lap Shear specimen)



Fig. 88:- Fracture image of 6 wt.% ultrasonically mixed composite (Lap Shear Specimen)

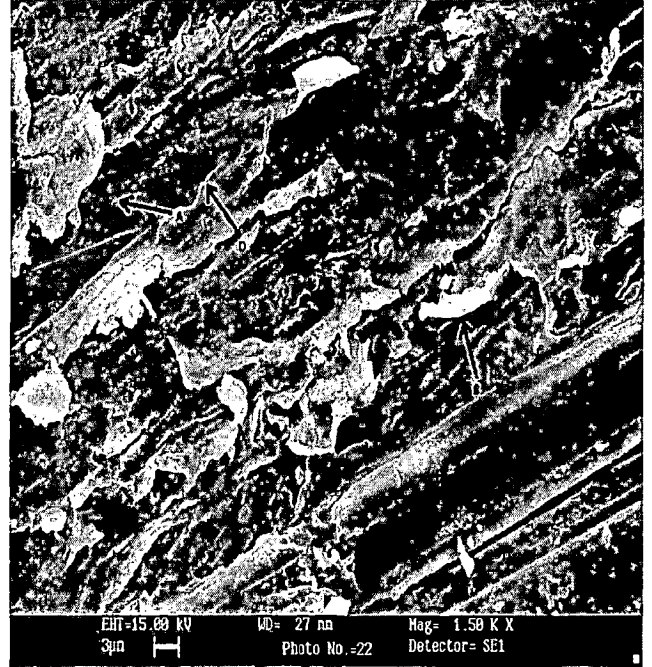


Fig. 89:- Fracture image of 8 wt.% ultrasonically mixed composite (Lap Shear specimen)



Fig. 90:- Fracture image of 10 wt.% ultrasonically mixed composite (Lap Shear Specimen)



Fig. 91:- Fracture image of 15 wt.% ultrasonically mixed composite (Lap Shear specimen)

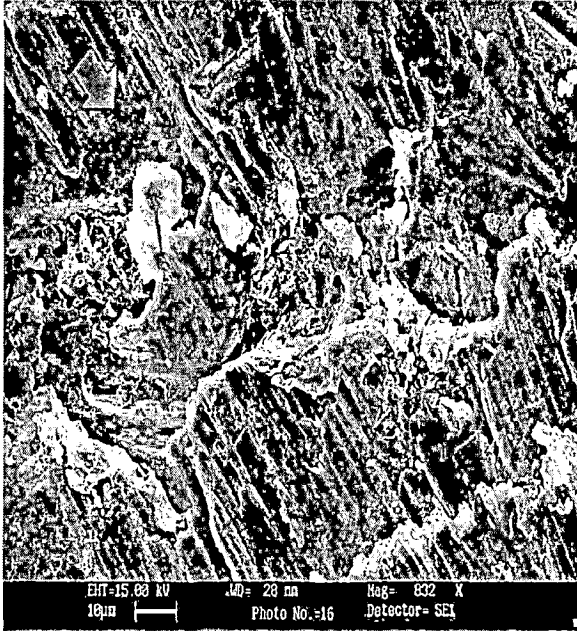


Fig. 92:- Fracture image of 20 wt.% ultrasonically mixed composite (Lap Shear Specimen)

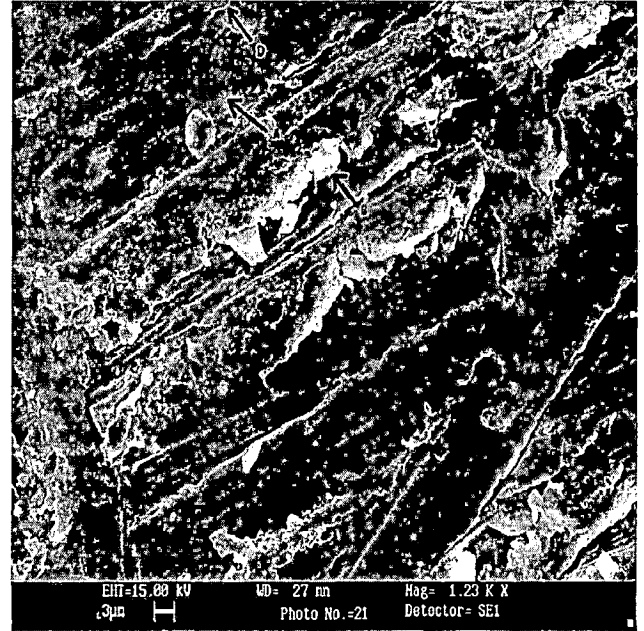


Fig. 93:- Fracture image of 20 wt% ultrasonically mixed composite (Lap Shear specimen) at 1230 X

Figure 68 for 8 wt.% filler addition by mechanical mixing shows that agglomerates of medium large size are showing poor bonding, medium agglomerates are showing partial bonding while small agglomerates show good bonding with the matrix which results in higher strength. Figure 69, 70 for 15 and 20 wt% respectively show smaller agglomerates exhibiting good bonding with matrix with absence of medium and large sized agglomerates, thereby showing more increment in strength.

Figure 74 shows fracture surface of 2 wt% filler added composite by ultrasonic method which shows crack pinning at nano particles and the growth direction. Similar effect can be seen in figure 75 and 76 for 5 and 6 wt% filler. Figure 77 shows fracture surface of 8 wt% composite at lower magnification while figure 78 shows effect of nano particles in assisting crack growth resistance. Similar results can be seen for 10 wt% composite in figure 79 and 80. In figure 81 and 82, the effect of filler on fracture behavior is not quite clear which also shows formation of typical C shape of nano particles when they are in large amount. Here they appear as separate particles but present in large amount. This effect is not quite clear. For 20 wt% filler composite the figure 83 shows very clear crack propagation direction and figure 84 shows the crack pinning effect. A crack propagating through a particle filled matrix will encounter the particles as obstacles and may be pinned. The crack front between the

obstacles moves on and extends by bowing so that the crack length increases. This particularly leads to a higher 'line energy' which is suggested to enhance the crack resistance [31]. Besides, secondary cracks and new fracture surface may be generated. Secondary cracks unify after passing an obstacle, and a fracture step may then be formed. Crack deflection processes at particle obstacles in a matrix have been proposed to play an important role in the toughening. The theory was described by Faber and Evans [29,30]. It is assumed that a crack can be deflected at an obstacle and that it is forced to move out of the initial propagation plane by tilting and twisting. Such deflection causes a change in the stress state from mode I to mixed-mode, e.g. mode I/II (tensile/ in-plane shear) in the case that the crack tilts, and mode I/III (tensile/anti-plane shear) if the crack twists. To propagate crack under mixed mode conditions requires a higher driving force than in pure mode I [29,30], which results in a higher fracture strength of the material.

Figure 85 shows the fracture surface of pure epoxy lap shear specimen which shows clearly the crack propagation direction and fracture of epoxy in purely brittle manner in an adhesive-cohesive manner. This feature is present in the entire lap shear specimens from 2 to 20 wt% filler addition as shown in figure 86 to 93. The figure 90 for 10 wt% filler composite shows fracture of adhesive in cohesive manner which justifies the strength increment for that particular sample. Figure 93 shows the adhesive fracture surface at the edge. It shows a large number of serrations along the thickness which indicates the large scale crack pinning and subsequent movement due to presence of nano particles. In the above figures of fracture surfaces A = apparent particles, B = plastic deformation, C = formation of cavities/debonding, D = shear banding and E = crack bridging.

#### 4.6 FOURIER TRANSFORM INFRARED SPECTROSCOPY RESULTS

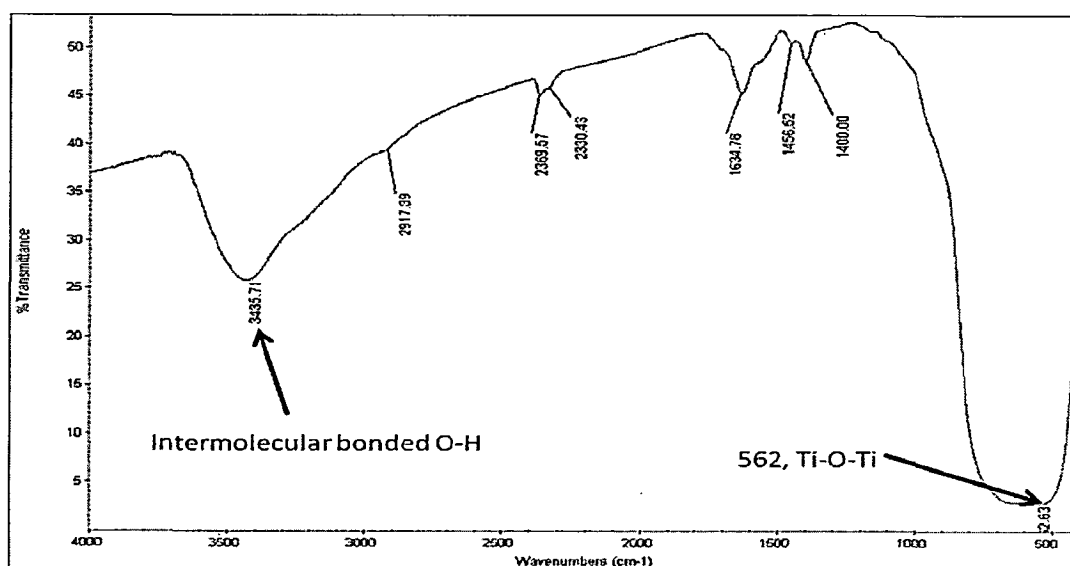


Figure 94:- FTIR of TiO<sub>2</sub> nano particles

Figure 94 shows FTIR plot for titanium dioxide particles. The peak at 562 wavenumber shows the presence of Ti-O-Ti. The same peak is present in all the FTIR plots of all composites. Figure 95 shows the details of the bond stretching and bending in pure polymer. Due to addition of Titanium dioxide particles no significant changes are seen in the bond vibrations in case of mechanical and ultrasonic mixing except the intensity of transmittance of 1509, 1249 and 821 wavenumbers are higher in ultrasonic mixed composite compared to mechanical mixed composite. 1509 wavenumber denotes the C – H bending vibration, while the 821 wavenumber denoted C – H out of the plane bending vibration. 1249 wavenumber is the asymmetric C – O – C stretching vibration.

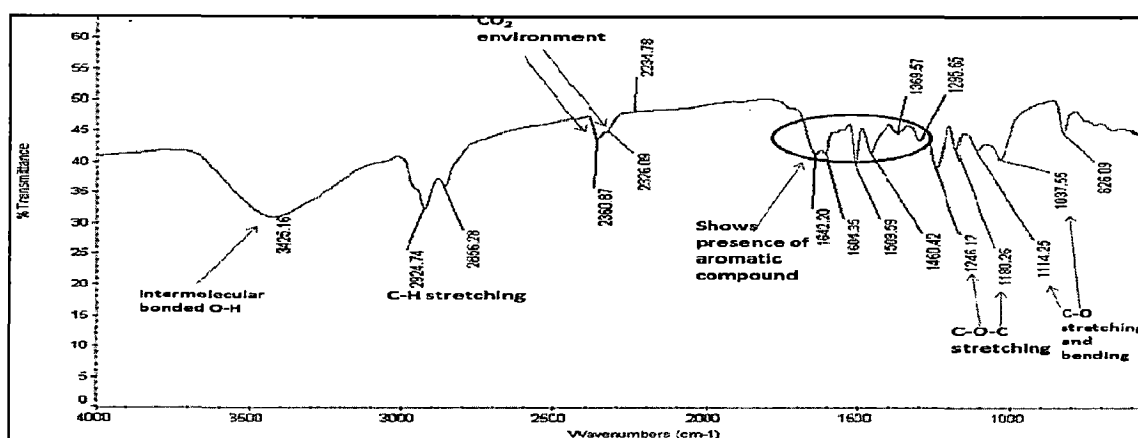


Figure 95:- FTIR of pure polymer

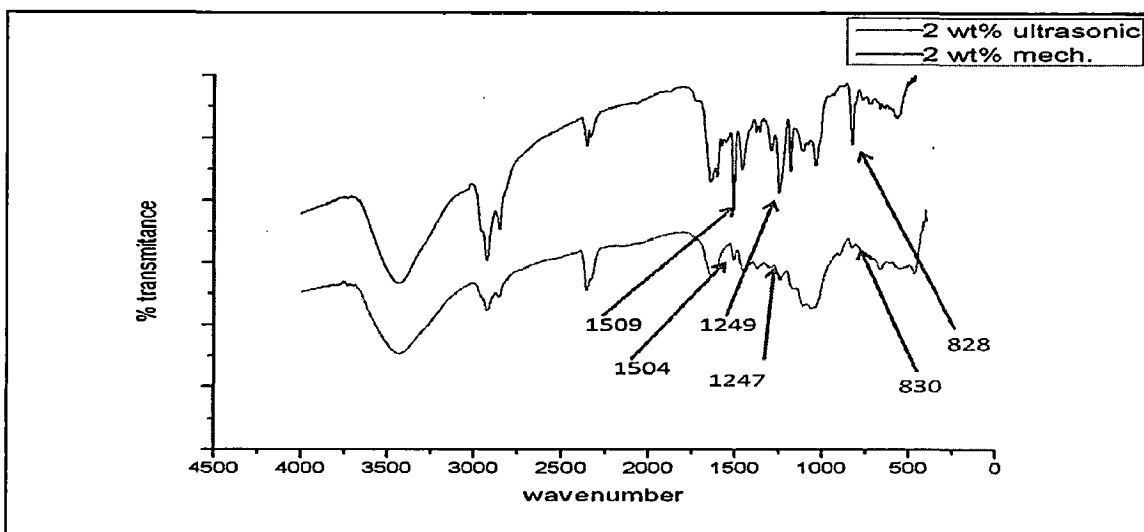


Figure 96:- FTIR of 2 wt% ultrasonic and mech. Mixed composite

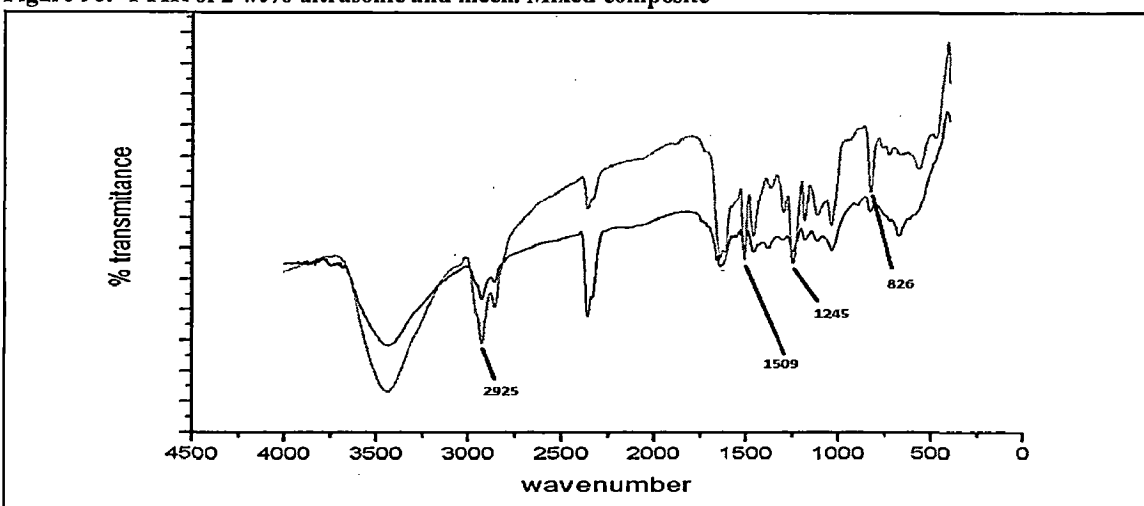


Figure 97:- FTIR of 4 wt% ultrasonic and mech. Mixed composite

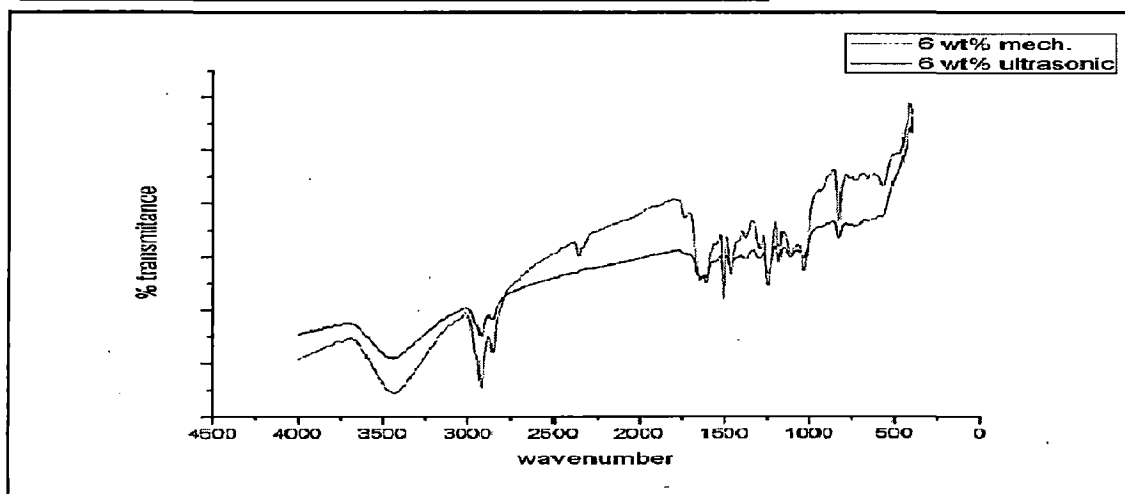


Figure 98:- FTIR of 6 wt% ultrasonic and mech. Mixed composite

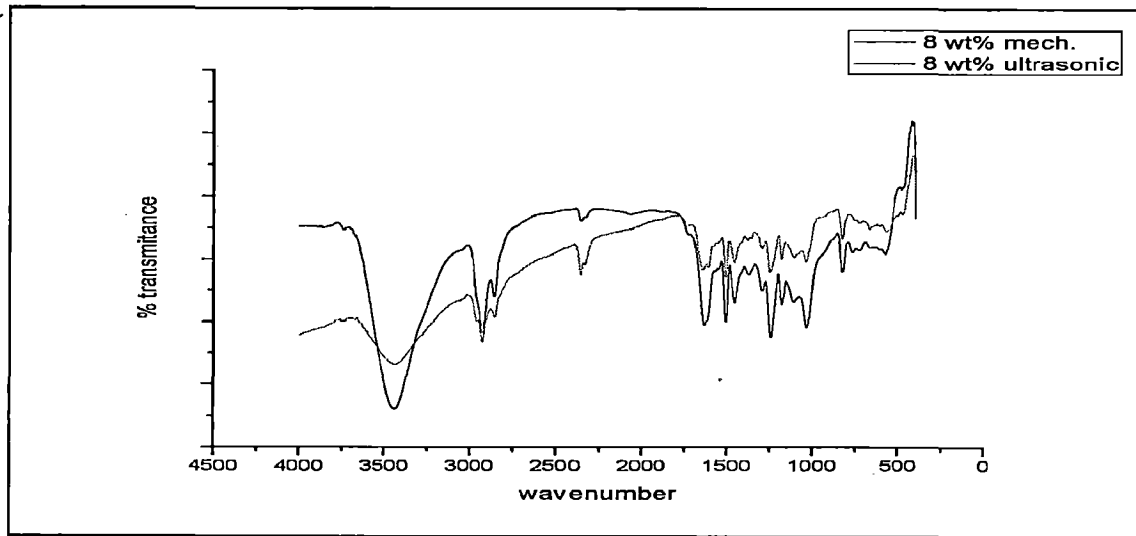


Figure 99:- FTIR of 8 wt% ultrasonic and mech. Mixed composite

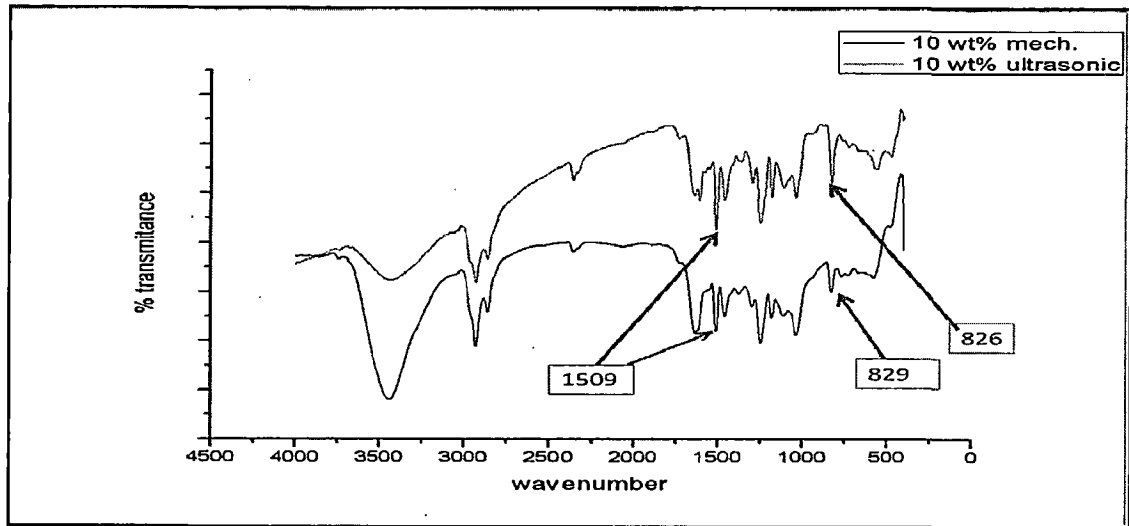


Figure 100:- FTIR of 10 wt% ultrasonic and mech. Mixed composite

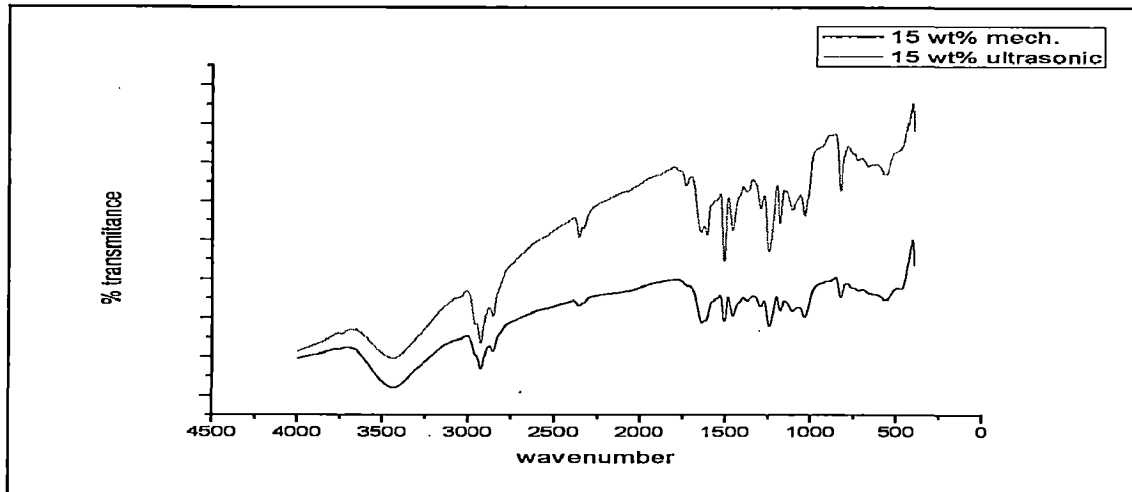


Figure 101:- FTIR of 15 wt% ultrasonic and mech. Mixed composite

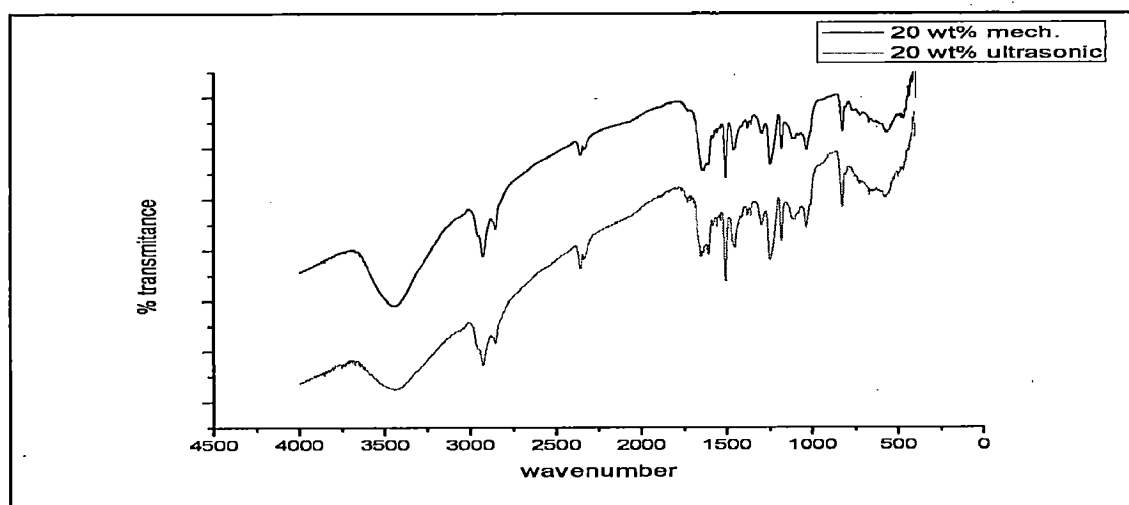


Figure 102:- FTIR of 20 wt% ultrasonic and mech. Mixed composite

The FTIR results of UV degraded pure adhesive and 20 wt% ultrasonically prepared composite adhesive show the following observations.

Type of bond	Pure polymer	UV Degraded pure polymer	UV Degraded 20wt% TiO <sub>2</sub> added composite
C – H Stretching, CH <sub>2</sub>	2924	2919, highly intense	2922, less intense
C – H Stretching, CH <sub>3</sub>	2856	2849, highly intense	2850, less intense
Carboxyl group	absent	1717	Absent
Aromatic compound	1460	1468, highly intense	1466, highly intense
-CH=CH- (Bending)	Absent	721, seen for 1 <sup>st</sup> time	721, seen for 1 <sup>st</sup> time

Table 12:- Comparison of pure and composite adhesive after UV degradation

The peak at 1717 is the carboxyl group formed from the epoxy chain leading to decrease in strength while the peak at 1721 observed for 20 wt% TiO<sub>2</sub> filled composite adhesive is carboxyl group from ketone. It has no effect on strength of composite. The peak at 721 shows rocking (Bending) of –CH=CH- bond, its effect on the strength or degradation is not clearly known.



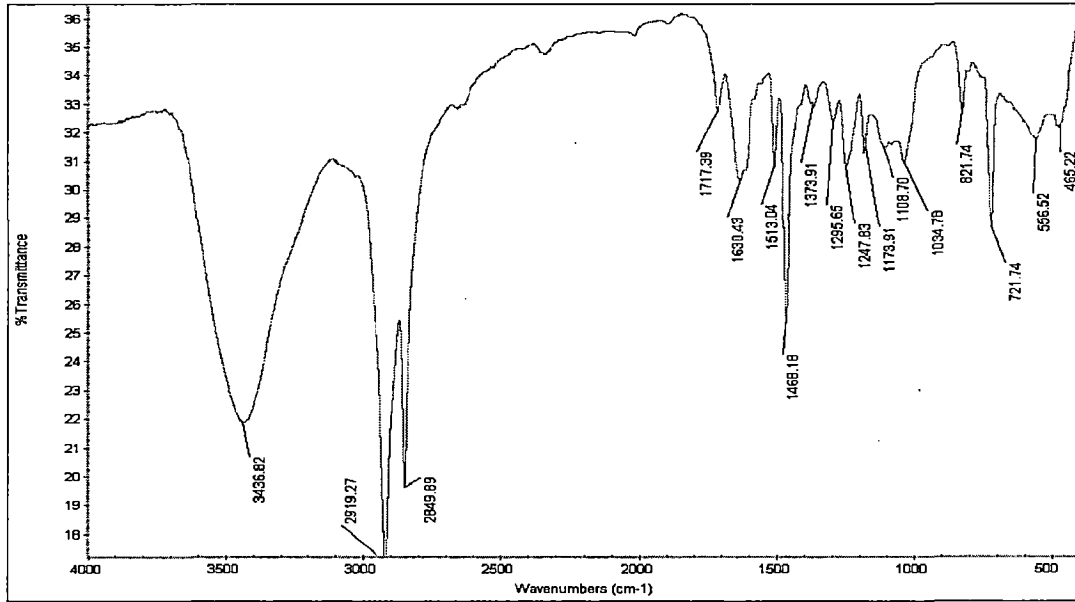


Figure 103:- FTIR plot of UV degraded pure polymer adhesive

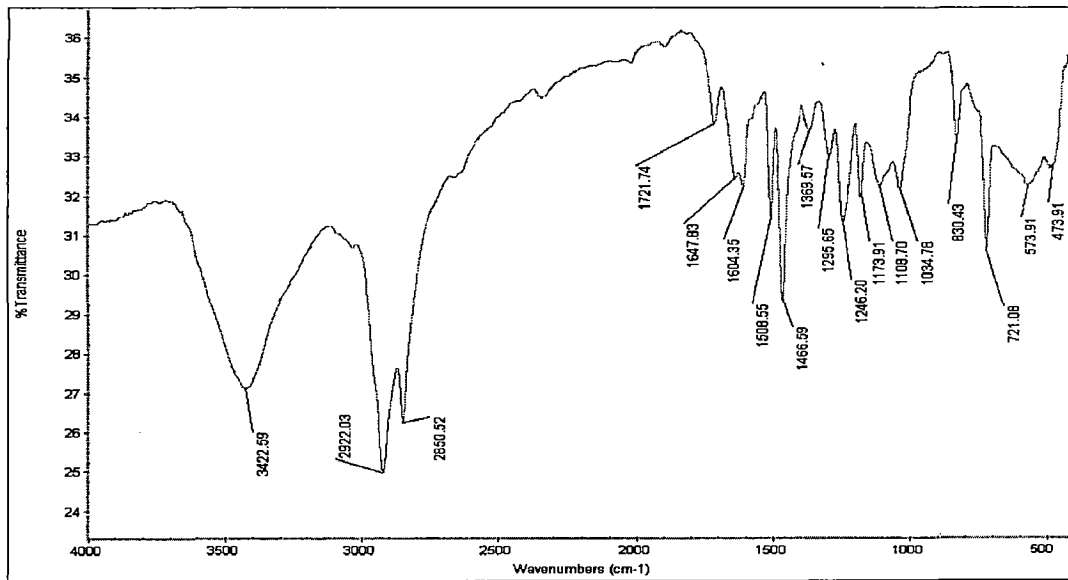


Figure 104:- FTIR plot of UV degraded 20 wt% TiO<sub>2</sub> ultrasonically mixed composite adhesive

#### 4.7 UV DEGRADATION TEST RESULTS

The UV degradation test result show that the strength of pure as well composite adhesive decreases with exposure time. The percentage decrease in strength of composite adhesive is lower compared to pure adhesive which justifies the effect of absorption of UV radiation by titanium dioxide nano particles. Figure 103 clearly shows the relationship between the percentage degradation of strength as a function of filler amount and exposure time.

Sample wt% TiO <sub>2</sub>	Tensile Strength (MPa) at different duration of exposure			
	0 days	8 days	16 days	24 days
0	20.89	20.07	19.02	17.83
10	30.65	29.82	28.46	27.06
15	33.89	32.46	31.62	30.71
20	35.08	34.56	33.56	33.02

Table 13:- Percentage decrease in strength of pure and composite adhesive as function of exposure time and amount of filler addition

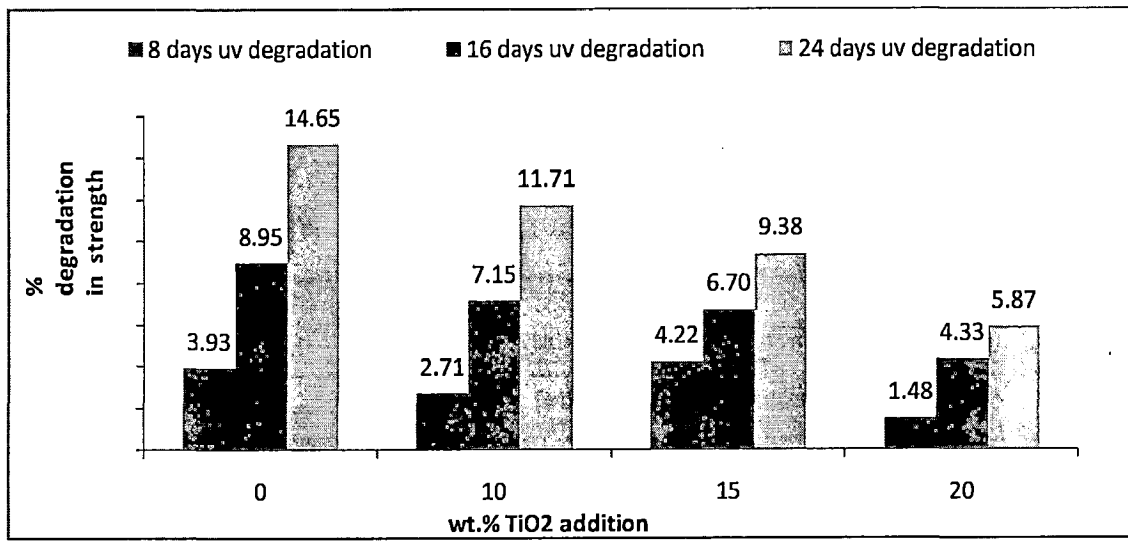


Figure 105 - Percentage degradation of strength as function of exposure days and amount of filler addition

## CHAPTER 5

## CONCLUSION

---

- Addition of TiO<sub>2</sub> to epoxy adhesive increases its tensile and lap shear strength. Highest strength values are obtained for 15 and 20 wt% addition of filler for both mechanical and ultrasonic mixing methods.
- Ultrasonic cavitation method is a very effective method to uniformly disperse nano particles in epoxy adhesive without use of any chemical reagent. The uniform dispersion of filler has appreciable impact on the overall properties of the composite.
- Addition of TiO<sub>2</sub> marginally increase the glass transition Temperature (T<sub>g</sub>) of epoxy adhesive while it appreciably enhances the IPDT, thereby increasing the thermal stability of the adhesive.
- The AFM results clearly show the formation of agglomerates of quite large size in mechanical mixing method while it shows uniform dispersion of nano particles in ultrasonic mixing method.
- The SEM results show poor interface adhesion between matrix and agglomerate in mechanically mixed samples while it shows good crack growth resistance offered by nano particles in ultrasonically mixed samples. Apart from crack pinning the other observed phenomena of fracture are crack deflection, chain scission, crazing, void formation.
- FTIR results show minor change in stretching or bending of bonds in pure polymer due to addition of nano fillers or due to ultrasonic mixing. UV degraded polymer shows presence of stressed carboxyl group at 1717 cm<sup>-1</sup> wavenumber which is the reason for poor strength of pure polymer while it is absent in the titania filled composite.
- The tensile strength results of UV degraded composite adhesive show that with increase in TiO<sub>2</sub> content, the reduction in strength decreases.

## CHAPTER 6 SCOPE FOR FUTURE WORK

---

- Characterization of the composite adhesive for high temperature applications is one of the fields which can be evaluated, as the thermal stability of pure epoxy is considerably improved by addition of titanium dioxide nano filler.
- The application of composite adhesive to UV LED lamp to practically characterize its UV resistance against pure epoxy.
- The application of composite in polymer solar cells can be investigated.
- The implementation of the composite as UV filter can be explored.
- The FTIR study shows intense peaks, shifting of peaks and appearance of new peaks. Work can be done to clearly interpret the effect of stress, UV degradation, ultrasonic cavitation and addition of nano particles on the bending and stretching vibrations of bonds.
- The composite may be used as a part of a system which converts UV light into visible light range and thus can be used in optical applications.

## CHAPTER 7

## REFERENCES

1. Spanoudakis, J. Young, R.J. Crack propagation in a glass particle filled epoxy resin Part 1: Effect of particle volume fraction and size. *J. Mater. Sci.* (1984); 19: 473–486.
2. Spanoudakis, J. Young R.J. Crack propagation in a glass particle filler epoxy resin Part 2: Effect of particle-matrix adhesion. *J. Mater. Sci.* (1984); 19: 487–496.
3. Moloney, A.C. Kausch, H.H. Stieger, H.R. The fracture of particulate-filled epoxide resins (part one). *J. Mater. Sci.* (1983); 18: 208–216.
4. Sahu, S. Broutman, L. Mechanical properties of particulate composites. *Polymer. Eng. Sci.* (1972); 12: 91–98.
5. Kinloch, A.J. Shaw, S.J. Tod, D.A. Hunston, D.L. Deformation and fracture behavior of a rubber-toughened epoxy: 1. Microstructure and fracture studies. *Polymer* (1983); 24: 1341–1354.
6. Yee, A.F. Pearson, R.A. Toughening mechanisms in elastomer modified epoxies: Part 1 Mechanical studies. *J. Mater. Sci.* (1986); 21: 2462–2474.
7. Kinz-Douglas, S. Beaumont, P.W.R. Ashby, M.F. A model for the toughness of epoxy-rubber particulate composites. *J. Mater. Sci.* (1980); 15: 1109–1123
8. Schadler LS, Brinson, LC, Sawyer WG. Polymer Nanocomposites. A small part of the story. *J of the Minerals, Metals and Materials Soc.* (2007); 59(3): 53-60.
9. Pablo Carballeira, Frank Hauptert. Toughening Effects of Titanium Dioxide Nanoparticles on TiO<sub>2</sub>/Epoxy Resin Nanocomposites. *Polymer Composites* (2009); DOI 10.1002/pc.2091:1 – 6.
10. R.M. Laine, J.W. Choi, and I. Lee. Organic/inorganic hybrid composites from cubic silsesquioxanes. *Adv. Mater.* (2001); 13: 800-810.
11. M.A.L. Machado, L. Valentini, J. Biagotti, and J.M. Kenny. Effect of processing technique on the dispersion of carbon nanotubes within polypropylene carbon nanotube-composites and its effect on their mechanical properties. *Polymer Composites.* (2009); 43: 1499-1504
12. A. A. Wazzan, H. A. Al-Turaif, A. F. Abdelkar. Influence of submicron TiO<sub>2</sub> particles on the mechanical properties and fracture characteristics of cured epoxy resin. *Polymer Plastics Technology and Engineering.* (2006); 45: 1155 – 1161
13. Wetzel B, Hauptert F, Friedrich K, Zhang MQ, Rong MZ. Impact and wear resistance of polymer nanocomposites at low filler content. *Polym Eng Sci.* 2002; 42 (9): 1919–1927.
14. Guijun Xian, Rolf Walter and Frank Hauptert. Friction and wear of epoxy/TiO<sub>2</sub> nanocomposites: Influence of additional short carbon fibers, Aramid and PTFE particles: *Composite Science and Technology.* (2006); 66: 3199 – 3209
15. Jordan J, Jacob KI, Tannenbaum, Sharaf MA, Jasiuk I. Experimental trends in polymer nanocomposites – a review. *Materials Science and Engineering* (2005); A393: 1-11.
16. Wang H, Tao X, Norton E. Optical properties of titanium dioxide nanoparticles/3-(2-benzothiazolyl)-7- N,N-diethylaminocoumarin/polymethyl methacrylate composite films. *Optical Materials* (2004); 27: 161- 166.
17. Mayer AC, Scully SR, Hardin BE, Rowell MW, McGehee MD. Polymer based solar cells. *Materials today* (2007); 10: 28-33.
18. Ou B, Li D, Liu Y. Compatibilizing effect of maleated polypropylene on the mechanical properties of injection molded polypropylene/polyamide 6/ functionalized- TiO<sub>2</sub> nanocomposites. *Composites Science and Technology* (2009); 69: 421-426.

19. Zou, J. Shi W, Hong X. Characterization and properties of a novel organic–inorganic hybrid based on hyper branched aliphatic polyester prepared via sol-gel process. *Composites Part A: Applied Science and Manufacturing*. (2005); 36: 631–637.
20. Abd-Rabou, M. Al-Turaif, H. Abdelkader, A.F. Friction and wear of sub-micron TiO<sub>2</sub>-filled epoxy coating under dry sliding conditions. *J. EGTRIB* (2004); 2: 17–24.
21. Yang, S.H., Nguyen, T.P., Rendu, P.L. Hsu, C.S. Optical and electrical properties of PPV=SiO<sub>2</sub> and PPV=TiO<sub>2</sub> composite materials. *Composites Part A: Applied Science and Manufacturing*. (2005); 36: 509–513.
22. C.B. Ng, L.S. Scbadler, and RW. Siegel. Synthesis and Mechanical Properties of TiO<sub>2</sub>-epoxy nanocomposites. In: *Proceedings of fourth international conference on nanostructured materials*. (1999); 12: 507 – 510.
23. MSDS Araldite 2011, Huntsman Advanced Materials.
24. Caseri WR. Nanocomposites of polymers and inorganic particles. preparation, structure and properties. *Materials Science and Technology* (2006); 22(7): 807-817.
25. Shao-Yun Fu, Xi-Qiao Feng, Bernd Lauke, Yiu-Wing Mai. Effects of particle size, particle/matrix interface adhesion and particle loading on mechanical properties of particulate–polymer composites. *Composites Part B: Engineering*. (2008); 39: 933 – 961
26. P.K. Ghosh, S.K. Nukala. Properties of Adhesive Joint of Inorganic nano filler composite adhesive. *IJEMS*. (2008); 15: 68 – 74
27. H.H. Kausch. *Polymer Fracture*. Springer – Verlag (1975); 251 - 306
28. Dale Ensminger. *Ultrasonics*. Marcel Dekker, Inc. (1973); 70-72
29. Faber KT, Evans AG. Crack deflection processes – I. Theory. *Acta Metall.* (1983); 31 (4): 565–576.
30. Faber KT, Evans AG. Crack deflection processes – II. Experiment. *Acta Metall.* (1983); 31(4):577–584.
31. Kinloch AJ, Maxwell D, Young RJ. Micro mechanisms of crack propagation in hybrid-particulate composites. *J Mater Sci Letter* (1985); 4: 1276–1279.
32. P.K. Ghosh. DST report “Progress Report to MHRD” MMED, IIT Roorkee, India. June 2010.
33. C.D. Dolye. *Analytical Chemistry*. (1961); 33: 77-84.
34. Manwar Hussain, Atsushi Nakahira, Shigehero Nishijima, Koichi Niihara. Fracture behavior and fracture toughness of particulate filled epoxy composite. *Elsevier Materials Letters*. (1996); 27: 21 – 25
35. K.S. Huang, Y.H. Hien, J.S. Chen, T.R. Shieh, J.W. Chen, “Synthesis and Properties of Epoxy/TiO<sub>2</sub> Composite Materials”; *Wiley Interscience DOI* (2006); 10.1002/pc20173: 195 – 200